Heat transfer, void fraction and pressure drop during condensation inside inclined smooth and microfin tubes

Adekunle O. Adelaja[1,2]*, Daniel R. E. Ewim[1], Jaco Dirker[1,]**, Josua P. Meyer[1,]***

[1]*Department of Mechanical and Aeronautical Engineering, University of Pretoria, Pretoria, Private Bag X20, Hatfield 0028, South Africa.*
[2]*Department of Mechanical Engineering, University of Lagos, Akoka Yaba Lagos*

**Corresponding Author:*

E-mail: josua.meyer@up.ac.za

Phone: +27 12 420 3104

***Alternative Corresponding Author:*

E-mail: jaco.dirker@up.ac.za

Phone: +27 12 420 2465

****Alternative Corresponding Author:*

E-mail: aadelaja@unilag.edu.ng

Highlights

- Effect of inclination during condensation inside smooth and microfin tubes.
- Void fractions predicted for inclined smooth and microfin tubes.
- Different inclination angles for maximum heat transfer in smooth and microfin tubes.
- Heat transfer enhancement found to be between 0.98 and 2.38.
- Pressure penalty factor found to be between 0.8 and 4.

ABSTRACT

This paper presents experimental heat transfer and pressure drop measurements during the condensation of R134a at a mean saturation temperature of 40 °C inside a microfinned copper tube with an inner diameter of 8.92 mm and a helix angle of 14°. Experiments were conducted for mean qualities from 0.1 to 0.9 at different inclination angles ranging from -90° (vertically downwards) to +90° (vertically upwards), at mass fluxes of 200 - 600 kg/m^{2}s. Heat transfer coefficients were calculated directly from measured data, while the frictional pressure drops were obtained from the experimental data using the Bhagwat and Ghajar void fraction correlation developed in 2014. Results were compared with those obtained from a similarly sized smooth tube having an inner diameter of 8.38 mm to obtain the relative microfin heat transfer enhancement and pressure penalty factors. For both tubes, it was found that the heat transfer coefficient increased significantly with the mean vapour quality and mass flux. For the microfin tube, the highest heat transfer coefficients were obtained at tube inclinations of between -15° and -5° (downward flows), while for the smooth tube, the highest heat transfer coefficients occurred between inclinations of between -30° and -15° (downward flows). The heat transfer enhancement factor for the microfin tube was between 0.98 and 2.38 depending on the inclination angle. For both tubes, it was found that higher frictional pressure drops occurred at higher mass fluxes. In most cases, higher vapour qualities produced higher frictional pressure drops depending on the flow pattern. The lowest frictional pressure drop occurred at either horizontal tube positions or vertical downward flow inclinations. Microfin pressure drop penalty factors ranged between approximately 0.8 and 4 depending on the mass flux, inclination and vapour quality.

Keywords: Condensation, heat exchanger, helical microfin tubes, inclined tubes, heat transfer enhancement, pressure penalty factor.

Nomenclature

A	area (m^2)
c_p	specific heat (J/kgK)
d	diameter (m)
e	fin height (m)
EB	energy balance
$E.F$	enhancement factor
g	gravitational acceleration (m/s^2)
G	mass flux (kg/m^2s)
h	enthalpy (J/kg)
H	helix angle (°)
k	thermal conductivity (W/mK)
L_t	heat transfer length of test section (m)
$L_{\Delta P}$	distance between pressure taps (m)
$\dot{m}$	mass flow rate (kg/s)
N	number of fins
n	number of thermocouples
Q	heat transfer rate (W)
P	pressure (kPa)
ΔP_{Tsat}	pressure difference between two saturation temperatures (kPa)
ΔP^*_{grav}	apparent gravitational pressure drop (kPa)
R	thermal resistance ($^oC/W$)
T	temperature (^oC)
x	vapour quality (-)
z	thermocouple position

Greek symbols

α	heat transfer coefficient (W/m^2K)
β	inclination angle (radian)
ε	void fraction (–)
ρ	density (kg/m^3)
$\rho*$	apparent density (kg/m^3)

Subscripts

a	actual

Cu	copper
fric	frictional
H_2O	water
i	inner
in	inlet
j	measurement location
lines	lines between pressure taps and transducer
l	liquid
m	mean/average
meas	measurement
mom	momentum
o	outer
out	outlet
pre	pre-condenser
ref	refrigerant
sat	saturation
stat	static
sys	system
test	test condenser
v	vapour
w	water
wall	wall

1. Introduction

Energy efficiency is imperative during the operation of heat exchangers and should be taken into consideration in the design phase. A wide range of industries such as the automobile, process, chemical, power production and refrigeration and air-conditioning industries are in constant need of improved heat transfer. Inclined heat exchangers however have a ready application in industrial A- and V-frame condensers; during banking, take-off and landing of aeroplanes and navigation of automobiles uphill and downhill. Research activities dedicated to enhancing heat exchanger efficiency by increasing heat transfer capacity in smaller and compact devices are therefore desirable. Heat enhancement techniques have been investigated and are broadly categorised into active and passive techniques. Among the passive techniques, the application of extended surfaces has attracted significant attention and has been implemented in many types of heat exchangers. One such application is the use of internally structured microfinned tubes, for which a large range of surface design types exist, including helical, cross-groove and herringbone microfinned tubes.

Several comprehensive works have been done on the heat transfer coefficients and the pressure drops in both smooth and microfin tubes [1-5]. Generally, the emphasis was on the heat transfer improvement and not all investigations necessarily considered the pressure drops penalty increase. Although pressure drop and heat transfer are often investigated independently, there is the need to have a holistic view of both variables for the sake of the design engineers who are end-users of the results. We need to maximise heat transfer and minimise pressure drops. Horizontal and vertical tube orientations have been studied extensively. However, there have been relatively few experimental works on inclined microfin tubes [6] or inclined smooth tubes [7-12], other than vertical flow orientations. Furthermore, to the best of our knowledge, there is a little reference in the open literature on the comparison of heat transfer coefficient, void fraction, and pressure drop in microfin tubes with those of smooth tubes at a wide range of inclination angles.

For the sake of an interested reader, the works on two-phase flow in microfin tubes are briefly reviewed. Common performance measures include that of the heat transfer enhancement factor and the pressure drop penalty factor. These are defined as the ratios between the microfin heat transfer coefficient or frictional pressure drop to the heat transfer coefficient or frictional pressure drop of a similarly sized smooth tube. Eckels and Pate [13] performed experiments during the condensation of R134a and R12 in a microfin tube with an inner diameter of 8.32 mm and a helix angle of 17°. It was found that the pressure penalty factors were lower than the heat transfer enhancement factors. However, for the condensation of R134a at the lowest saturation temperature and highest mass flux, the pressure drop penalty factor slightly exceeded the heat transfer enhancement factor. Chamra et al. [14] considered the condensation and evaporation of R22 in helical microfin and cross-groove microfin tubes with various helix angles. They found that for condensation, the pressure penalty factor generally increased with the helix angle, while for evaporation, it was minimised at a helix angle of 17.5°. Eckels et al. [15] reported that for the condensation of R22, R134a, R410a and R407C in microfinned tubes of helix angle of 18°, the pressure drop increased with an increase of either the vapour quality or the mass flux, but decreased with saturation temperature. Their data indicated maximum penalty factors at a mass flux of 250 kg/m^2s, while average vapour qualities of 50% resulted in minimised penalty factors. Cavallini et al. [16] studied the condensation of a number of refrigerants (pure refrigerant, azeotropic and zeotropic) in horizontally oriented helical and cross-groove microfinned tubes. They compared their heat transfer and pressure drop data with existing correlations and found them to be in good agreement. Miyara et al. [17] studied the effect of fin height and helix angle on the heat transfer and pressure drop in horizontal herringbone microfin tubes. It was found that an increase in the helix angle resulted in increased heat transfer coefficients and pressure drops. For fin heights below 0.18 mm, it was found that the heat transfer coefficients and pressure drop values increased as the fin height increased. However, above this height, there was only a negligible heat transfer coefficient enhancement, while the pressure drop continued to increase. Nualboonrueng and Wongwises [18] considered the pressure drop characteristics of R134a in smooth and microfin tubes. They observed heat transfer coefficients of between 10% and 85% higher in the

helical microfin tubes as compared with smooth tubes of the same inner diameters. Their enhancement and penalty factors exhibited similar trends for each tube at the same experimental conditions. Olivier et al. [19] compared the thermal performance of helical and herringbone microfin tubes with a smooth tube in a horizontal orientation during the condensation of R22, R407C and R134a at an operating temperature of 40 °C. Inlet quality ranging between 85% and 95% and outlet quality ranging between 5% and 15% were considered for mass fluxes between 400 kg/m^{2}s and 800 kg/m^{2}s. The tests showed that the herringbone and helical finned tubes had pressure gradients that were about 79% and 27% higher than those of the smooth tube. Han and Lee [20] carried out an experimental study on condensation heat transfer enhancement and pressure drop penalty factors in four microfin tubes with diameters of 8.92 mm, 6.46 mm, 5.1 mm and 4 mm with R22, R410A and R134a as the refrigerants. They investigated the effect of vapour quality and mass flux and found that the penalty drop factors increased with vapour quality but decreased after reaching the upper limit of 0.6. They attributed this to the turbulence generation from the microfin tubes explaining that with an increase in vapour quality, microfins extruded over the liquid film and caused a slight increase in the frictional losses in the medium (0.4-0.6) vapour quality region. However, in the high vapour quality region, the turbulence level was so high that contribution to turbulence generation by the extruded microfins decreased with vapour quality. For the heat enhancement factor, they noted that R410A had the lowest value of the three refrigerants tested and they further found that the average heat enhancement factors were lower than unity at the higher mass flux region, which implied that microfins could be more effective in the lower mass flux region. They also proposed correlations for condensation frictional pressure drop and heat transfer coefficients for the annular flow regime of their study. Honda et al. [21] studied the condensation of R407C in horizontal microfin tubes for a saturation temperature of 40 °C, mass fluxes between 50 kg/m^{2}s and 300 kg/m^{2}s, and condensation temperature differences of 1.5 °C, 2.5 °C and 4.5 °C. They considered the effects of the mass velocity and condensation temperature difference and developed a new heat transfer correlation to cater to the trends found in their study. Liebenberg and Meyer [22] investigated the condensation of R22, R407C and R134a in horizontal smooth and microfin tubes with an inner diameter of 8.9 mm. They found

that the microfin tube heat transfer coefficient was twice that of the smooth tubes. The heat transfer enhancement factor and pressure drop penalty factor showed a similar trend at certain vapour qualities and mass fluxes. The local and average pressure drop penalty factors were found to be higher than the local and average heat transfer enhancement factor respectively. In some cases, they obtained enhancement factors less than unity, especially at low vapour qualities. Olivier et al. [23] investigated the heat transfer, pressure drop and flow patterns in horizontal tubes during the condensation of R22, R407C and R134a at a saturation temperature of 40 °C in smooth, helical and herringbone microfin tubes for mass fluxes between 400 kg/m^{2}s and 800 kg/m^{2}s, for condenser inlet and outlet vapour qualities of between 85% and 95%, and 5% and 15% respectively. As compared with the smooth tube, the heat transfer coefficients were 70% higher for the herringbone and 40% higher for the helical microfin tube. They also developed a two-phase multiplier type of correlation for the frictional pressure drop by assuming that the liquid-only friction factor was not only of a function of Reynolds number but also dependent on the physical geometry of the tube and the effects of the fin. Akhavan-Behabadi et al. [6] reported on the condensation of R134a in a microfin tube with different tube orientations and asserted that inclination angle, vapour quality and mass flux significantly affected the heat transfer. They considered relatively low mass fluxes of 54 kg/m^{2}s, 81 kg/m^{2}s and 107 kg/m^{2}s, at mean vapour qualities between 20% and 80%, and at saturation temperatures ranging between 26 °C and 32 °C. The effect of the inclination was found to be more significant at low quality and low mass flux wherein gravity forces were dominant. The optimum inclination angle, resulting in the highest heat transfer coefficient, was reported to be +30° (upward flow). Kim et al. [24] studied the adiabatic pressure drop during the condensation of carbon IV oxide in horizontal and vertical smooth and microfin tubes with mean inner diameters of 3.48 mm and 3.51 mm respectively at saturation temperatures of between -25 °C and -15 °C. They reported that the frictional pressure drop characteristics of the vertical flow were much different from those of the horizontal flow. They concluded that the microfin tube did not always have a superior in-tube condensation performance in terms of enhancement factor and pressure penalty factor. Sapali and Patil [25] investigated the condensation of R134a and R404a at high condensing temperatures (55-65 ^{o}C). The experiments were

carried out in a horizontal smooth tube with an inner diameter of 8.56 mm and a microfin tube with an inner diameter of 8.96 mm. They found that the heat transfer coefficient for R134a was greater than that for R404a and that the microfin tube thermally outperformed the smooth tube. The heat transfer coefficient enhancement factor for R134a was between 1.5 and 2.5, while that of R404a was between 1.3 and 2.0. In another paper by the same authors [26], they considered microfin U-tubes and found that as the saturation temperature was increased between 35 °C and 60 °C, the frictional pressure drop decreased by up to 23.5% and 45.6% in the smooth tube and the corresponding microfin tube respectively. Colombo et al. [27] considered the flow pattern, heat transfer and pressure drop for evaporation and condensation of R134a in two horizontal microfin tubes. The "HVA" tube (larger numbers of fins) and the "VA" tube (fewer numbers of fins) gave higher heat transfer coefficients and pressure penalty factors when compared with the smooth tubes. However, the behaviour of these tubes differed depending on whether an evaporation or condensation process was of interest. During condensation, the "HVA" microfin tube had a lower thermal performance compared with that of the "VA" tube. Adelaja et al. [11] investigated the condensation of R134a in an inclined microfin tube with an inner diameter of 8.92 mm and a helical angle of 14° at a saturation temperature of 40 °C. The results were compared with those of an inclined smooth tube having an inner diameter of 8.38 mm. The heat transfer enhancement factor obtained was between 1.07 and 2.38 and depended on the inclination angle. Besides this, little other references to studies conducted at different inclination angles could be found for microfin tubes. Wu et al. [28] performed experiments during the convective condensation of R410A inside a smooth tube with an inner diameter of 3.78 mm and six different microfin tubes with fin root diameters of 4.54, 4.6 and 8.98 mm. Their working mass fluxes were from 99 to 603 kg/m^{2}s. It was found that the heat transfer enhancement increased as the mass flux decreased. They explained that the heat transfer enhancement mechanism in microfin tubes was mainly due to the surface area increase at large mass fluxes, while liquid drainage by surface tension and interfacial turbulence enhanced heat transfer greatly at low mass fluxes. They compared the results of their experiments with those of the models of Cavallini et al. [29], Kedzierski and Goncalves [30], Chamra et al. [31] and Yu and Koyama [32] and found that they could predict the

results of their experiment within an error band of ±30%. Zhang et al. [33] conducted a numerical study on the heat transfer characteristics of condensation for R410A inside horizontal microfin tubes with 0° and 18° helical angles. They found that the local heat transfer coefficients increased with increase in mass flux, vapour quality and helical angle. Surprisingly, they also found that the heat transfer enhancement in the helical microfin tubes was more pronounced at higher mass flux and vapour quality. Li et al. [34] performed experiments to determine the heat transfer characteristics during the condensation of R22 and R410A in a horizontal smooth tube and microfin tubes of different diameters. It was found that the heat transfer coefficient (HTC) of the microfin tube was 1.65 to 2.55 times that of the smooth tube. It was also found that the microfin tube yielded approximately 30% higher pressure drops than for the smooth tube. With respect to the different tube diameters, it was found that the 5 mm diameter tube had higher heat transfer coefficients and pressure drops than the 9.52 mm diameter tube. Zhang et al. [35] conducted an experimental study of R410A condensation heat transfer and pressure drop characteristics in microfin and smooth tubes with an outer diameter of 5 mm. Their mass flux ranged from 390 to 1583 $kg/m^2 s$ with different saturation temperatures of 309.15 K, 316.15 K and 323.15 K. It was found that the heat transfer coefficients and pressure gradients increased with increasing mass flux. It was also found that lower saturation temperatures led to higher heat transfer coefficients and pressure drops. They also asserted that the heat transfer enhancement ratios of microfin tubes ranged from 1.28 to 1.65. They concluded by asserting that the heat transfer enhancement ratios decreased with increasing mass fluxes and saturation temperatures. Bashar et al. [36] performed experiments to determine the heat transfer coefficients and pressure drops during the condensation of R134a inside a small diameter microfin and smooth tube at low mass flux conditions. It was found that the frictional pressure drop, as well as the condensation heat transfer coefficient, increased with mass flux and vapour quality. It was also found that the pressure drop was higher in the microfin tube compared with the smooth tube with the same experimental condition. The pressure drop penalty factor range was 1.01 to 2.11. The heat transfer coefficients were higher in the microfin tube for all mass fluxes and were about 2 to 5 times greater than those of the smooth tube at a mass flux of 100 kg/m^2s. Sun and Li [37] developed a

correlation for predicting frictional pressure drop during condensation inside horizontal microfin tubes. They collected a database of 481 data points, covering nine refrigerants including CO_2 at average condensation temperatures ranging from 14 to 65 °C. The mass velocities considered and average vapour qualities ranged from 50 to 800 kg/m^{2}s and 0.11 to 0.91 respectively. Four available correlations were used to evaluate the experimental results at hand It was found that the Cavallini et al. [38] model had the best prediction performance predicting 85.6% of the collected data points within an accuracy of ±30%. They leveraged on this to develop a new correlation based on the Martinelli parameter modified by incorporating the reduced pressure. It was found that this new model showed good agreement with valuable data. Finally, some corresponding experimental work was conducted for evaluating the reliability of their new model. Yang et al. [39] performed heat transfer and pressure drop experiments during the condensation of R410A with vapour flowing upwards in a smooth tube with an inner diameter of 8.32 mm and a microfin tube with a fin root diameter of 8.76 mm. Measurements were taken at saturation temperatures of 40 ^{o}C, 45 ^{o}C and 48 ^{o}C with mass fluxes in the range of 80 to 345 kg/m^{2}s. It was found that the condensation heat transfer coefficients increased with the increase of mass flux for both smooth and microfin tubes, apart from at low mass flux in the smooth tube where the condensation heat transfer coefficients decreased with the increase of cooling heat flux. With respect to the heat transfer enhancement factors, it was found that they were higher with an increase in saturation temperature (1.3-2.05) at saturation temperature of 40 ^{o}C and (1.4-2.2) at saturation temperature of 48 ^{o}C. The pressure drop penalty factors were in the ranges of (1.0-1.6) at saturation temperature of 40 ^{o}C and (1.03-.5) at saturation temperature of 48 ^{o}C. The results of their experiments were compared with some well-known heat transfer correlations for microfin tubes. It was found that the correlation suggested by Chamra and Mago [40] showed the best agreement with the results with an average deviation of 31%. Based on their experimental data, two revised correlations for condensation heat transfer and frictional pressure drops for microfin tubes were proposed, within ±15% and ±25% accuracy respectively. Li et al. [41] performed convective condensation experiments for three enhanced tubes with an outer diameter of 9.52 mm with different surface modifications. Measurements were taken at mass flux values ranging from 70 to 330 kg/m^{2}s at

a constant saturation temperature fixed at 313 K; with an inlet quality of 0.9 and an outlet quality of 0.2. They reported a heat transfer enhancement factor of between 1.4 and 1.65 for one of their novel enhanced tubes with a corresponding penalty factor of 2.9 to 4.0. They explained that this high penalty factor was a result of increased friction, turbulence and fluid obstruction due to the dimples and petal arrays used to manufacture the enhanced tube. Most recently, Pham et al. [42] presented new experimental data and developed a new correlation for R32, R22 and R410A undergoing condensation inside a horizontal enhanced tube at a saturation temperature of 48 ^{o}C. However, pressure drops were not reported.

Several works have been published by Meyer and his co-researchers dealing with heat transfer coefficient in smooth inclined tubes. For example, Lips and Meyer [7, 8] and Adelaja et al. [43] investigated condensation heat transfer in inclined smooth tubes at different inclination angles between vertical downward flow (-90°) and vertical upward flow (+90°) at saturation temperature of 40 °C. Adelaja et al. [11] conducted their experiment at a saturation temperature of 50 °C, while Meyer et al. [10], in addition to inclination angles, studied the effect of saturation temperature on the heat transfer coefficients. Therefore, it can be concluded that even though there is data available for smooth inclined tubes, there is a need to conduct additional studies to investigate the heat transfer enhancements and pressure drop penalty factors during convective condensation inside horizontal and inclined enhanced tubes.

In this paper, we present new experimental heat transfer, void fraction, and pressure drop data for microfin tubes, which may assist in narrowing the gap in the literature in this regard. Measured condensation heat transfer coefficients for a new inclined microfin tube with a helix angle of 14° were obtained for R134a at a saturation temperature of 40 °C for mass fluxes ranging from 200 kg/m^{2}s to 600 kg/m^{2}s, and inclination angles ranging from -90^{o} to +90^{o}. The results were compared with earlier results presented on smooth tubes. This enabled the calculation of the enhancement factor and the investigation thereof with respect to the mean vapour quality, mass flux and inclination angle. In addition, the experimental pressure drop, the recorded flow patterns, the associated predicted void fraction based on correlations from literature, and the pressure penalty factors were studied with

respect to the inclination angle, mean vapour quality and mass flux in microfin and smooth circular tubes.

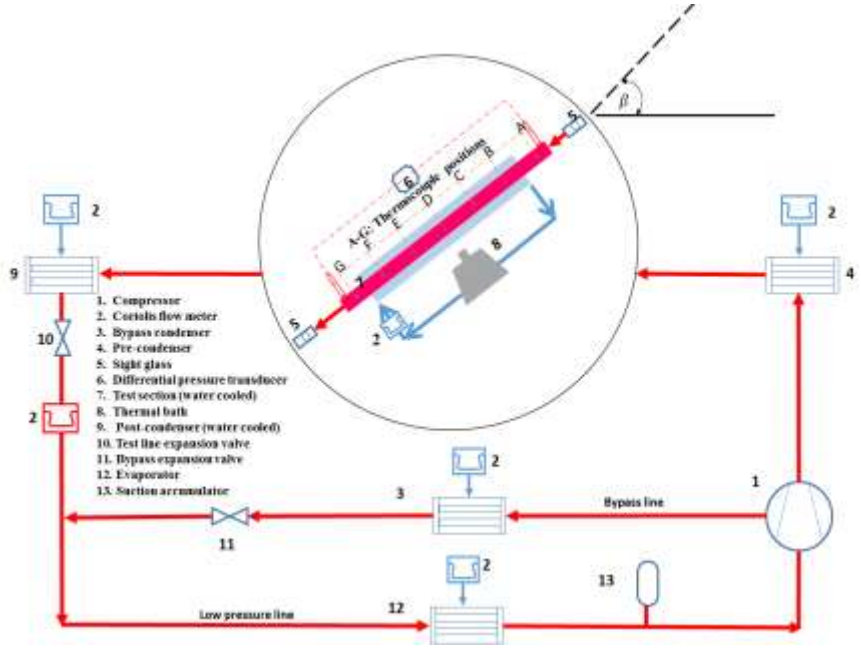

Fig. 1a. Schematic diagram of the experimental setup.

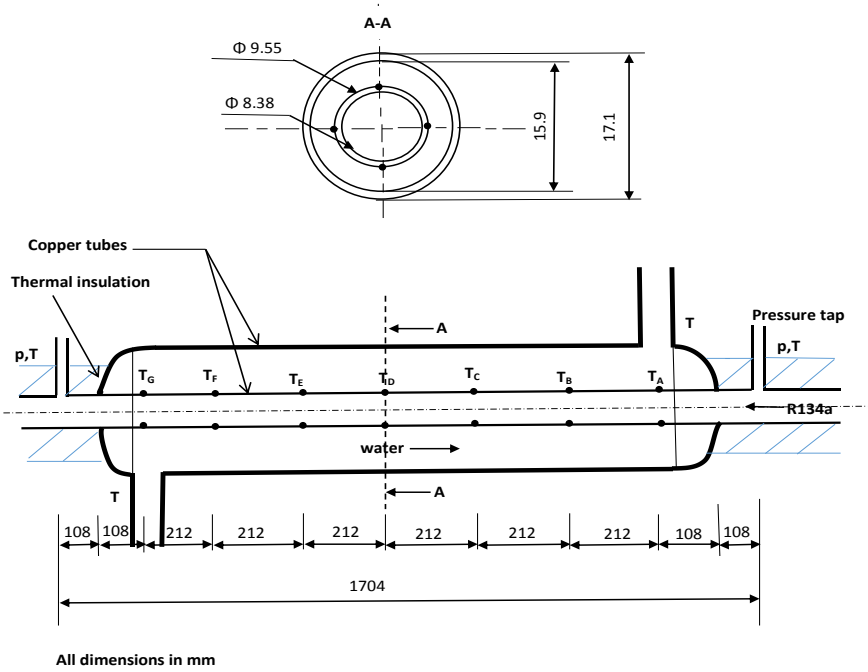

Fig. 1b. Schematic diagram of the test section.

2. Experimental apparatus

The test bench (Fig. 1) used for the investigation was well established and had previously been used for condensation studies [4, 7, 8, 10-12, 22, 23, 43-55]. In these works, comprehensive descriptions and explanations were given. However, a short overview is presented in this paper. As shown in Figs. 1a and 1b, the test facility consisted mainly of a refrigerant loop operated as a vapour compression cycle with several water loops servicing the condensers and the evaporator.

2.1. Refrigerant loop

Refrigerant R134a was circulated through the vapour-compression loop by a hermetically sealed scroll compressor, which had a cooling load rating of 10 kW. The loop had two high-pressure lines (the test line and a bypass line) and one low-pressure line. Electronic expansion valves were used to control the refrigerant flow in each of the high-pressure lines.

The refrigerant test line contained three water-cooled condensers in series, namely the pre-condenser, the test condenser and the post-condenser as well as a Coriolis mass flow meter (CFM010), which had a measuring accuracy of ±0.35%. The pre-condenser was used to regulate the inlet vapour quality to the test condenser by adjusting the pre-condenser water flow rate. The post condenser, which followed the test condenser, was used to fully condense and sub-cool the refrigerant in the test line. The bypass line, which also contained a water-cooled condenser, was used to control the mass flow rate, temperature and pressure in the test line. Directly after the expansion valves, the test line and bypass line joined. Following the junction, the low-pressure line contained a water-heated evaporator and a suction accumulator.

Two test condensers were considered (one with a smooth tube and the other with a microfin tube). Both were counterflow tube-in-tube heat exchangers constructed from hard-drawn copper such that each had a heat transfer length of L_t = 1.488 m. The inner tubes were equipped with pressure port locations located (one location at the inlet and the other at the outlet) $L_{\Delta P}$ = 1.704 m apart. Refrigerant

passed through the inner tube, while water flowed in the annulus. The inclination angle, β, of the particular test condenser could be adjusted (see Figure 1) between +90° (upward refrigerant flow) and -90° (downward refrigerant flow).

For the smooth tube heat exchanger, the inner tube had a measured outer-wall diameter of d_o = 9.55 mm and a measured inner-wall diameter of d_i = 8.38 mm. For the microfin tube heat exchanger, a commercial microfin tube was used, which had the same measured outer diameter of d_o = 9.55 mm, a slightly different inner diameter of d_i = 8.92 mm and a helix angle of 14° (also see Figure 2). More detailed geometric information about the smooth and microfin tubes is supplied in Table 1. For both test condensers, the outer tube of the heat exchanger was smooth with an inner-wall diameter of 15.9 mm.

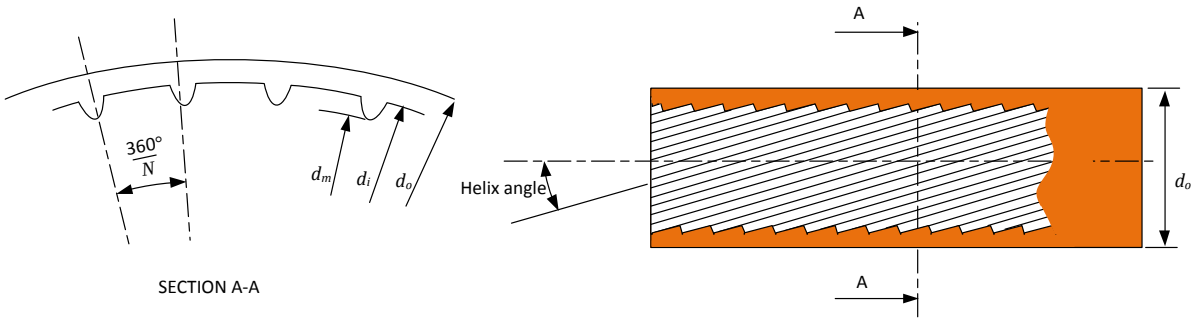

Fig. 2. Geometry of the microfin tube (adapted from Thome [70]).

Table 1: Geometry of the tubes.

Description	Value	
	Microfin	Smooth
Outer diameter d_o [mm]	9.55	9.55
Inner diameter d_i [mm]	8.92	8.38
Mean inner diameter d_m [mm]	8.71	
Wall thickness [mm]	0.32	0.598
Fin height e [mm]	0.21	
Fin pitch [mm]	0.445	
Circumferential fin number, N [-]	60	
Helix angle H [°]	14	
Roughness (e/d_i)	0.0235	

Three pressure ports were located at each pressure port position at the inlet and the outlet. Two pressure ports at the inlet and two at the outlet were connected to two separate pressure transducers to obtain the absolute pressures before and after the test section. The other two ports (one at the inlet and the other at the outlet) were connected to a differential pressure transducer, which was used to directly measure the pressure difference between the inlet and the outlet during condensation. Care was taken to ensure that the pressure tap holes into the test section had no burrs. The pressure tap hole diameter was 0.77 mm, and was, therefore, less than 10% of the tube diameters, as recommended by Rayle [56]. The differential pressure transducer was calibrated to an accuracy of $\pm$0.05 kPa, while the other pressure transducers had an accuracy of ±2 kPa for low mass fluxes (100 kg/m^{2}s-200 kg/m^{2}s) and ±12 kPa for high mass fluxes (greater than 300 kg/m^{2}s). The pressure hoses were made of nitrile, reinforced with two high-tensile steel wire braids and covered with synthetic rubber. The differential pressure measuring lines were heated between the pressure taps and the transducer such that the line temperature was kept at about 5 to 10°C above the saturation temperature so that only vapour was present in them. The heating elements used for this were controlled with a LabVIEW program.

In-line connection points were used to connect the relevant test condenser into the test line. Sight glasses were positioned directly before and after the test condenser. These enabled flow visualisation and also served as thermal insulators against axial heat conduction. A high-speed camera was installed at the outlet sight glass and was used to record and document the flow patterns. Good colour fidelity was achieved by using a backlight with an evenly distributed light-emitting diode illumination. To ensure that the inlet refrigerant flow to the tubes was not influenced by upstream bends, a straight calming section, 50 diameters long, was situated before the inlet sight glass, as suggested by Van Rooyen [57].

For each test condenser, the inner-wall temperatures were measured with 28 T-type thermocouples embedded into the inner-tube wall (Fig. 1b). The thermocouples were distributed along the length and the circumference of each particular test section in groups of four thermocouples each, at seven equidistant stations. The thermocouples were soldered into drilled pot holes positioned at the top,

bottom and either side of the tubes. The thermocouple leads were passed through the annulus. The inlet and the outlet refrigerant saturation temperatures were measured with sets of three thermocouples each, at the inlet and the outlet of each test condenser. In each set, these thermocouples were positioned at the top, bottom and one side on the external surface of the tubes. All the thermocouples used were calibrated against a high-precision Pt-100 resistance temperature detector with an uncertainty of 0.1 °C.

The consistency of the saturation temperature readings was checked by comparing the saturation temperatures acquired from the thermocouples with the saturation temperatures associated with the average measured absolute pressure, obtained at the inlet and the outlet, using REFPROP [58]. The difference in the indirectly obtained saturation temperature and the average of the measured saturation temperature values was found to be less than 0.1 °C at high mass fluxes (400 kg/m^{2}s and above), while a slightly higher variation was observed at low mass fluxes.

Flexible hoses were used to connect the tilting portion of the test line into the refrigerant loop. The hoses were also insulated with polyethylene pipe insulation to reduce heat loss. Likewise, all other components in the refrigerant loop were thermally well insulated.

2.2. Water loops

As mentioned, the condensers and the evaporator were cooled and heated via cold and warm water loops respectively. The cold and warm water loops each had a 5 000 *l* insulated tank individually equipped with a 70 kW heating and a 50 kW cooling dual-function heat pump respectively. These pumps were thermostatically controlled such that the cold and warm water temperatures were set to be 10 °C and 25 °C respectively. In order to determine the heat transfer rates in the pre- and post-condensers (which were needed for data processing), the water inlet and outlet temperatures, as well as the water mass flow rates in these heat exchangers, were measured. Water inlet and outlet temperatures were obtained at each heat exchanger by using two thermocouples at each location.

Water flow rates were obtained using Coriolis mass flow meters (CFM010 and CFM025), which each had a measuring accuracy of 0.1%. As with the refrigerant loop, all thermocouples on the water sides were also calibrated.

Table 2: Test parameters and range.

Parameter	Range	Band
T_{sat} [°C]	40	± 0.6
G [kg/m^{2}s]	200, 300, 400, 600*	± 5
x_m [-]	0.1– 0.9 (as highlighted below)	± 0.01
	0.25, 0.5, 0.75 (for G = 200 kg/m^{2}s)	
	0.1, 0.25, 0.5, 0.75, 0.9 (for G = 300 kg/m^{2}s)	
	0.25, 0.5, 0.75, 0.9* (for G = 400 kg/m^{2}s)	
	0.5* (for G = 600 kg/m^{2}s)	
β [°]	0°, ±5°, ±10°, ±15°, ±30°, ±60°, ±90°	± 0.1
Q_{H2O} [W]	230 - 270	± 20
ΔP [kPa]	-2 to +12	±0.05

* This data is only for the microfin tube.

3. Experimental method

Table 2 contains the parameter set considered in this paper. For the microfin condenser, 169 combinations of refrigerant mass fluxes between 200 kg/m^{2}s and 600 kg/m^{2}s, mean vapour qualities between 0.1 and 0.9, and test section inclination angles between vertical downward flow and vertical upward flow were tested for a saturation temperature of 40 °C. For the smooth tube condenser, 143 combinations were tested. Therefore, this paper reports on experimental data gathered for 312 different cases in total. Tests were conducted with heat transfer rates of between 230 W and 270 W, which were used to control the span of the vapour quality in the test section. The change in the vapour quality (from the inlet to the outlet) ranged linearly from approximately 0.13 at a mass flux of 200 kg/m^{2}s to 0.044 at 600 kg/m^{2}s. Test conditions were meticulously set up by adjusting the

refrigerant mass flow rates via the electronic expansion valves and by also carefully selecting the water flow rates in the pre-condenser, test condenser, post-condenser and bypass condenser.

Data from the thermocouples, pressure transducers and Coriolis flow meters were collected by a computerised data acquisition system. The system consisted of a desktop computer on which was installed a LabVIEW program written to automatically acquire needed data, an analogue/digital interface card, shielded cable assembly, signal-conditioning extensions for instrumentation, transducer multiplexers, terminal blocks, channel multiplexers and termination units. The user interface displayed all measurements as well as some primary and secondary calculated quantities. This included the combined energy balance error (*EB*) of the pre-condenser, test condenser and post-condenser by comparing the refrigerant heat transfer rate, Q_{ref}, with the water heat transfer rate, Q_w:

$$EB = \frac{\left|Q_{ref} - Q_w\right|}{Q_{ref}} \tag{1}$$

Once the system was at steady state and the combined energy balance error was below 3%, the different sensor signals were recorded continuously through the data acquisition system for a period of two minutes at 1 Hz (121 data points). In order to avoid noise measurement, the arithmetic average of each data acquisition channel was used for the calculations of the fluid properties, heat transfer coefficients and other parameters of interest.

The oil concentration in the refrigerant was determined by Suliman *et al.* [50] in a former work within our research group using the ASHRAE Standard [59] and was determined as 1.8% on average. The maximum measured was 2.3% and only occurred at much higher mass fluxes of 700 kg/m^2.s, which greater than the range considered in this study. In their study, the presence of oil was shown to have a negligible effect on the results presented.

4. Data reduction

In this section, an overview of the heat transfer data reduction method is supplied. First, the method used to obtain the mean vapour quality in the test condenser is described; where after the methods for calculating the convective heat transfer coefficient and the frictional pressure drop are given.

The magnitude of the refrigerant heat transfer rate in the pre-condenser, and/or test condenser and/or post-condenser can be generically expressed as follows:

$$Q_{ref} = \left| \dot{m}_{ref} \left(h_{in} - h_{out} \right) \right| \tag{2}$$

Here, $\dot{m}_{ref}$ is the refrigerant mass flow rate obtained from the test line Coriolis refrigerant mass flow meter and $h_{in}=h_f + x_{in}h_{fg}$ and $h_{out}=h_f + x_{out}h_{fg}$ are the relevant refrigerant inlet and outlet specific enthalpies. Likewise, the magnitude of the water heat transfer rate can also be obtained:

$$Q_w = \left| \dot{m}_w c_p \left(\overline{T}_{w,in} - \overline{T}_{w,out} \right) \right| \tag{3}$$

Here, $\dot{m}_w$ is the water mass flow rate obtained from the relevant water loop Coriolis mass flow meter, C_p is the specific heat capacity evaluated at the average bulk fluid water temperature and $\overline{T}_{w,in}$ and $\overline{T}_{w,out}$ are the arithmetic average temperature readings at the relevant water inlet and outlet points.

The inlet enthalpy of the refrigerant at the pre-condenser was obtained via REFPROP at the measured saturation temperature and absolute pressure at the inlet. The outlet enthalpy of the pre-condenser was calculated with equation (2) based on the heat transfer rate recorded from the water side of the pre-condenser using equation (3). Because the test line was well insulated between the pre-condenser and the test condenser, the inlet enthalpy of the test condenser was equal to the outlet enthalpy of the pre-condenser. By reapplying the energy balance principle via equations (2) and (3) to the test condenser, the outlet enthalpy for the test condenser was determined. Based on the enthalpy values at the inlet and the outlet of the test condenser, the inlet and the outlet vapour qualities were obtained from the saturation properties at the measured inlet refrigerant temperature. The mean vapour quality (x_m) was calculated as the arithmetic average of the inlet and the outlet vapour qualities.

The average heat transfer coefficient (α) in the inner tube was calculated from Newton's law of cooling as follows:

$$\alpha = \left| \frac{Q_{test}}{A(\overline{T}_{wall,i} - \overline{T}_{sat})} \right| \tag{4}$$

where, in the case of the microfin tube, $A = \pi d_m L_t$ and for the smooth tube $A = \pi d_i L_t$. $\overline{T}_{sat}$ is the mean refrigerant saturation temperature obtained from the arithmetic average of the measurements taken at the inlet and the outlet of the section. $\overline{T}_{wall,i}$ is the mean inner-wall temperature and was determined from the average outer-wall temperature ($\overline{T}_{wall,o}$) by taking into consideration the radial heat conduction in the tube wall. The average outer-wall temperature on the inner tube was calculated using the trapezoidal numerical integration: radial heat by taking into consideration the

$$\overline{T}_{wall,o} = \frac{1}{L_t} \sum_{j=1}^{6} \left[\left(\overline{T}_{w,o}^{\,j} + \overline{T}_{w,o}^{\,j+1} \right) \left(z_{j+1} - z_j \right) \right] \tag{5}$$

where $\overline{T}_{wall,o}^{\,j}$ is the circumferential average temperature at the j^{th} location positioned at an axial distance of z_j from the test section inlet.

Based on the overall pressure difference between the inlet and the outlet pressure ports of the test condenser (ΔP_{test}), the frictional pressure drop component (ΔP_{fric}) can be determined by taking into consideration the kinetic energy and the potential energy of the fluid. This can be written as prescribed by Ould Didi et al. [60] as follows:

$$\Delta P_{test} = \Delta P_{stat} + \Delta P_{mom} + \Delta P_{fric} \tag{6}$$

The potential energy effect is represented by the static pressure drop (ΔP_{stat}) and the kinetic energy effect is represented by the momentum pressure drop (ΔP_{mom}). ΔP_{test} was determined from the measured pressure difference at the differential pressure transducer (ΔP_{meas}) by accounting for the inclination effect of the test condenser via the static pressure difference in the pressure lines (ΔP_{line}), which connected the differential pressure transducer with the inlet and the outlet pressure ports:

$$\Delta P_{meas} = \Delta P_{test} + \Delta P_{line} \tag{7}$$

The static pressure difference effect due to the vapour that was trapped in the pressure lines was calculated as follows:

$$\Delta P_{line} = \rho_v g L_{\Delta P} \sin\beta \tag{8}$$

Here, the vapour pressure density (ρ_v) was determined from REFPROP at the measured saturation pressure. This is approximately correct because the pressure lines were maintained only about 5 to 10 °C above the saturation temperature. β was the measured inclination angle of the test section, obtained with a digital inclinometer calibrated to an accuracy of $\pm 0.01^{o}$.

The static and momentum pressure difference in equation (6) was calculated as follows:

$$\Delta P_{stat} = \rho_{tp} g L_{\Delta P} \sin\beta \tag{9}$$

$$\Delta P_{mom} = G^2 \left[\left(\frac{(1-x_m)^2}{\rho_l (1-\varepsilon)} + \frac{x_m^2}{\rho_v \varepsilon} \right)_{out} - \left(\frac{(1-x_m)^2}{\rho_l (1-\varepsilon)} + \frac{x_m^2}{\rho_v \varepsilon} \right)_{in} \right] \tag{10}$$

Here, ρ_{tp} is the assumed homogeneous two-phase density given in equation (11), ρ_l is the saturated liquid-phase density obtained from REFPROP, G is the mass flux determined from the measured mass flow rate and the inner-tube cross-sectional area and ε is the vapour void fraction in the inner tube.

$$\rho_{tp} = \rho_l (1-\varepsilon) + \rho_v \varepsilon \tag{11}$$

Because both the static pressure and the momentum pressure differences are dependent on the void fraction, ε is an important parameter to determine. Several experimental investigations have been conducted to measure the void fraction for various flow pattern regimes. Also, several models have been developed to correlate the void fraction to measurable quantities such as the phase temperatures and the dimensions of the flow passage. These models were mostly developed for horizontal and/or vertical tube orientations [61-63] and can be categorised into three types: slip models, *k-α* models and drift-flux models. Only a limited number of studies focusing on inclined tubes have been conducted [45, 64]. Because most of the experimental conditions in this study were at flow orientations other than vertical or horizontal flow, the drift-flux model proposed by Bhagwat and Ghajar [64] was

adopted in this paper. Because of its non-linearity, the equations used in this model were solved iteratively until the predicted void fraction converged.

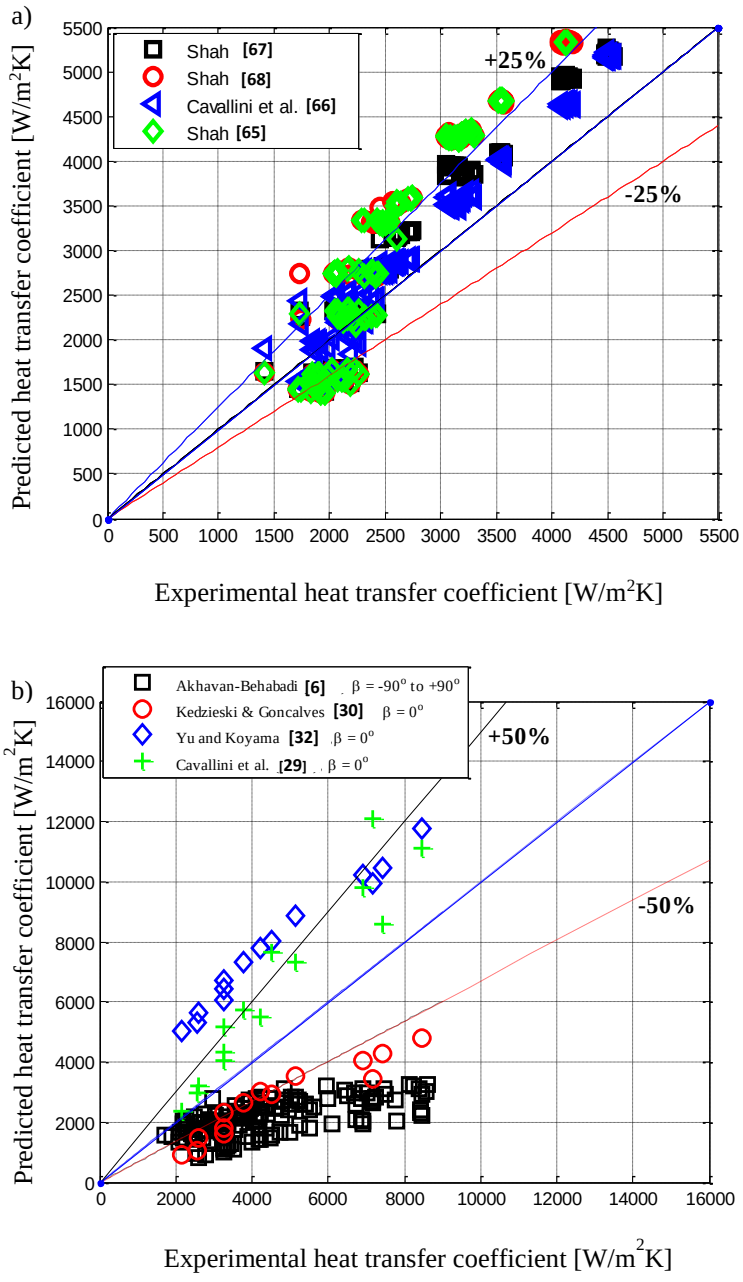

Fig. 3. Comparison of experimental data for heat transfer coefficient with some predictive models for a) the smooth tube and b) the microfin tube.

5. Data comparison with existing correlations

5.1. Heat transfer coefficients

Before the experimental results are presented, the heat transfer coefficients obtained from this experimental study is compared with some well-established correlations in Fig. 3a, for smooth tube data and in Fig. 3b, for microfin data.

Smooth tube data and literature correlations were compared in some of our previous works [10, 11]. However, in the present paper, a new correlation formulated by Shah [65] for inclined tubes is also added along with three other correlations to evaluate the smooth tube data. This is shown in Fig. 3a. It can be seen that the correlation by Cavallini et al. [66] had the best agreement with the experimental heat transfer coefficients, followed by the Shah [67] correlation of 1979. The models of Shah [65, 68] are very similar in their predictions.

Despite the effort invested to identify suitable heat transfer correlations, only one was found for condensation in inclined microfin tubes, while several were found for condensation in horizontal microfin tubes. Of these, a few have been chosen and are used here. The correlation by Akhavan-Behabadi et al. [6], developed for inclined microfinned tubes, is used as a comparison for all of the data points, while the correlations by [30, 32, 69] are only used for comparison for horizontal tube orientations as presented in Fig. 3b. It can be seen that only a few of the predicted data points fall within the ±50% error band. It can be noted that the correlation by Akhavan-Behabadi et al. [6] underpredicts most of the data, especially for high mass fluxes. This may be due to the fact that the correlation was developed for low mass fluxes between 54 kg/m^{2}s and 107 kg/m^{2}s and saturation temperatures between 26 ^{o}C and 32 ^{o}C. In terms of the other correlations (which were specifically developed for horizontal enhanced tubes), the correlation by Kedzierski and Goncalves [30] underpredicts the data, while the correlations by Yu and Koyama [32] and Cavallini et al. [69] overpredicts the data.

Among these, the correlation by Cavallini et al. [69] produces predictions with the best agreement with the experimental data. Based on these comparisons, it can be concluded that none of the models is adequate to predict the data. Based on the lack of agreement between the correlation predictions and the experimentally obtained data, there is, therefore, a need for an improved correlation, but this is not the focus of this study.

5.2. Void fraction

Smooth tube void fraction values were measured by Olivier et al. [45] on the same test bench and smooth tube test section used in this study. Therefore, the details of the void fraction measurement can be seen in the article and not repeated here. In Fig. 4, a comparison is given between the predictions of several smooth tube void fraction correlations from literature against their experimental data. Only horizontal flow conditions are considered in this figure. The models and correlations included are the homogeneous model [70], and the correlations of [63, 64, 71-74]. It can be seen that most of the predicted void fraction values are within ± 30% of the experimentally obtained values. The mean deviations from the experimental data of each prediction method are -29.3% for the homogeneous model, +6.3% for Zivi [71], +9.4% for Wallis [72], +2.2% for Rouhani and Axelsson [63], +15.5% for Chen [73], +6.3% for Yashar et al. [74], and +7% for Bhagwat and Ghajar [64]. All the correlations except that of Bhagwat and Ghajar were specifically developed for horizontal tube orientations. Of these, the Wallis correlation has the best performance. However, because the current investigation includes the impact of the tube orientation, the Bhagwat and Ghajar prediction method is of special interest in this article. In order to account for the influence of the microfins, it is needed to adjust the predicted void fraction value to take into consideration the smaller cross-section flow area due to the presence of the microfins. According to [75-77], the void fraction of the microfin tube is approximately 95% of that of a smooth tube. This is because the fraction of the cross-sectional area of the fin represents approximately 5% of the tube cross-sectional area. According to Wilson [74], a void fraction of 95% or less will result in liquid film thicknesses that cover the entire fin.

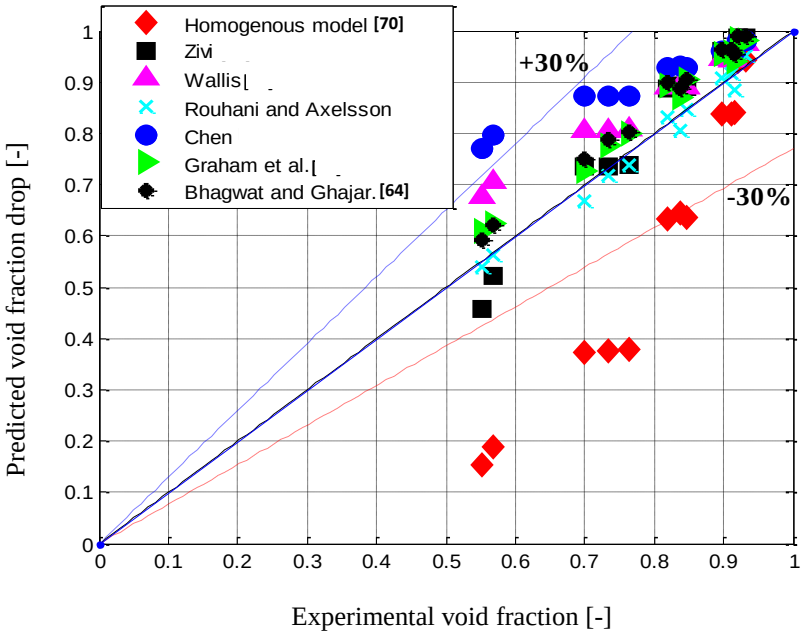

Fig. 4. Comparison of the predicted void fraction models for horizontal tube orientation with the calculated void fraction from Olivier et al. [45] experimental data for microfin tube.

Due to the lack of experimental void fraction data for microfin tubes, the smooth tube experimental data of Olivier et al. [45] was multiplied by 0.95 for comparison purposes with the Bhagwat and Ghajar and apparent void fraction correlations. Fig. 5 gives a comparison of the predicted void fraction from the method as well as the calculated apparent void fraction of Lips and Meyer [8] against the adjusted experimental data of Olivier et al. [45] for inclined tubes (covering all experimental data between β = -90° and +90°). It should be noted that for the apparent void fraction to be correct, the frictional pressure drops for the inclined orientation must be the same as those for the horizontal orientation.

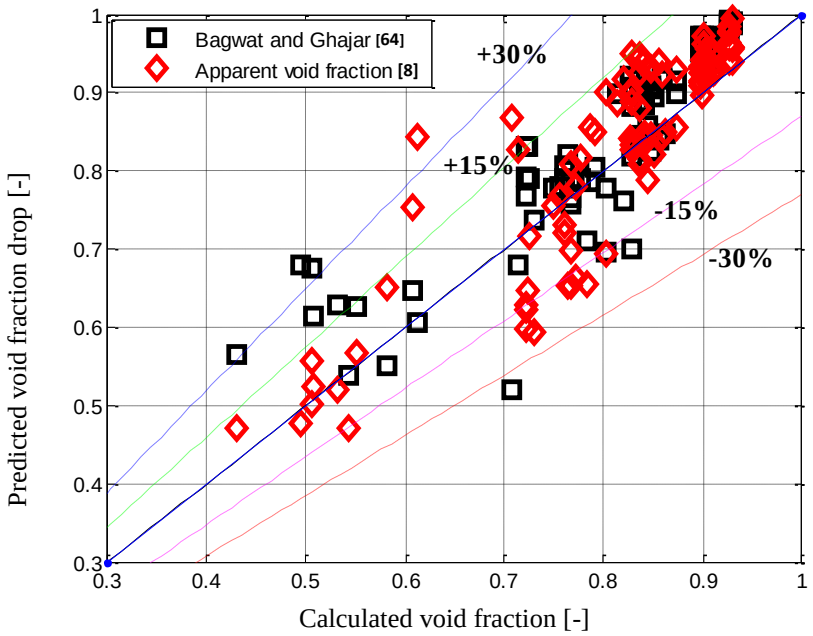

Fig. 5. Comparison of the apparent void fraction model [8] and Bhagwat and Ghajar [64] with the calculated void fraction for inclined tube orientation.

This is not necessarily true as is revealed later in this article and should be specifically checked. The apparent void fraction is therefore only included here for an order-of-magnitude comparison. From Fig. 5, it can be seen that almost all the inclined tube void fractions were predicted within ± 30% of the experimental values. The mean deviations of the Bhagwat and Ghajar method and the apparent void fraction are 7.5% and 6.6% respectively. If a multiplier of 0.96 instead of 0.95 is used, the mean deviation for the Bhagwat and Ghajar method and apparent void fraction predictions are 6.7% and 6.1% respectively. Thus, better agreement is obtained with a slightly lower multiplier. However, for the remainder of this article, the Bhagwat and Ghajar void fraction prediction method is adopted with a multiplier of 0.95.

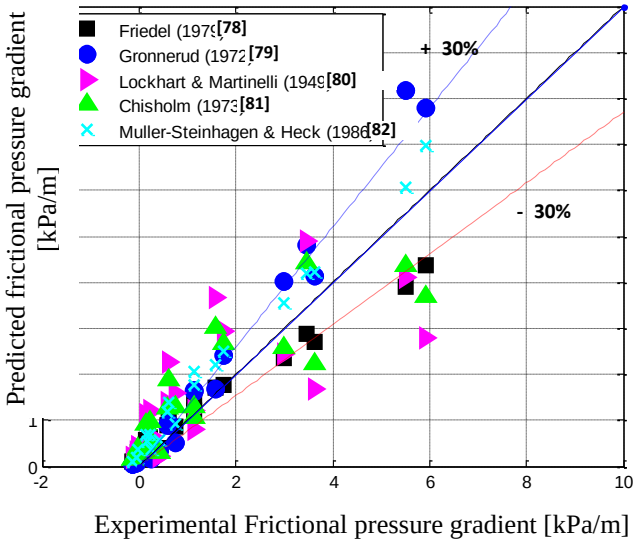

Fig. 6a. Comparison of smooth tube frictional pressure gradient with different correlations for horizontal flow.

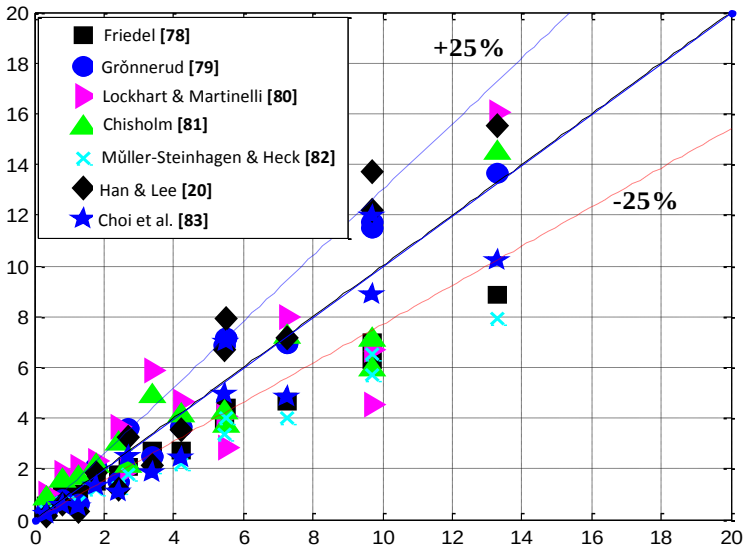

Fig. 6b. Comparison of microfin tube frictional pressure gradient with different correlations for horizontal flow.

5.3 Frictional pressure gradient

Pressure drop largely depends on the thermo-physical properties of the fluid, the mean vapour quality, the mass flux, the inclination angle and the saturation temperature. To validate or check the authenticity of our experiment, our experimental test data was compared with well-established and tested models. Fig. 6a shows the comparison of horizontal orientation experimental data for a smooth

tube with the models of Friedel [78], Grönnerud [79], Lockhart and Martinelli [80], Chisholm [81], Muller-Steinhagen and Heck [82] while Fig. 6b shows the result of the horizontal orientation experimental data in comparison with seven frictional pressure drop prediction models of Friedel [78], Grönnerud [79] Lockhart and Martinelli [80], Chisholm [81], Muller-Steinhagen and Heck [82], Han and Lee [20], Choi *et al*. [83]. Most of the data points are within close proximity of 30% and 25% error band for the smooth and microfin tubes respectively, confirming the integrity of the experimental data. In Fig. 6a, within the region of positive pressure gradient, the experimental results are in good agreement with the models while in the negative pressure gradient range they all failed. Müller-Steinhagen and Heck [82] appeared to be the best followed by the duo of Friedel [78] and Grönnerud [79]. The phenomenon of negative frictional pressure gradient ($\Delta P_{fric}/L$) is scarce in the open literature.

Few researchers, however, reported that the phenomenon occurs in two-phase flow at low liquid mass flow rate [84-87]. Cornwell and Kew [88] observed that at low mass fluxes. there was instability in the flow and that corresponds to Taylor bubble flow while Nicklin [89] attributed it to an occasion when the total pressure became lower than the hydrostatic pressure. Termed complete flow reversal [85, 89, 90], it is said to occur as a result of slip between the vapour and liquid at the interface when the liquid mass flow rate is low. Consequently, the local backward flow of the liquid results in wall shear stresses that act opposite the usual sense.

6. Experimental results

6.1. Underlying phenomena

In order to properly interpret the results, the mechanism associated with heat transfer enhancement in inclined microfin tubes needs to be well understood. The mechanism can be elucidated in four perspectives: the increment in the effective area, the draining of condensate through the grooves by the action of surface tension, the turbulence generated in the liquid film by the fins, and the prevailing flow pattern.

Because of the increased internal surface area of the microfinned tube compared with that of a smooth tube, any superficial enhancement of heat transfer rate must be checked against the increased surface area, as will be done later in this article. During condensation in a microfin tube, the formed condensate is drained from the tip of the fin through the combined effect of centrifugal and surface tension forces into the spiral groove. Thereafter, the vapour shear and/or gravity forces drive the liquid in the downward direction. These actions promote and prolong the range of or tendency for annular flow, which is associated with the generally observed increased heat transfer coefficient and pressure drop [91]. However, for different inclinations of the tube, the condensate both in the groove and above the fins is subjected to the gravitational force.

When the fin height protrudes above the liquid, a drain surface tension effect is established. This increases both the heat transfer rate and pressure drop as vapour makes contact with the fins. When the fins are completely covered by the condensate film, the effect of surface tension is reduced but turbulence is initiated by the effect of the fin. Therefore, the effect of surface tension is more pronounced in high vapour quality flows [20, 91].

In addition, the heat transfer performance and frictional pressure drops in inclined microfin tubes can be significantly influenced by the inclination angle. This has been shown to have a remarkable influence on the flow pattern when considering, for instance, smooth circular tubes [7, 8, 10-12, 44] and a microfin tube [12]. During downward flow, due to the action of gravitational force in the direction of the flow, the condensate film becomes thinner, thus resulting in increased void fractions. If the fins protrude above the film, as is the case of high vapour quality, a surface tension force is established at the vapour, fin and condensate interface. This leads to an increase in the heat transfer and pressure drop. On the other hand, during upward flow, the condensate film becomes thicker, which reduces the void fraction, increases the thermal resistance, hence, the heat transfer coefficient.
The interfacial force at the vapour-condensate interface causes additional turbulence. With the thicker film, the fins are submerged under the condensate and the surface tension becomes reduced. The

predominant forces, in this case, are the gravitational and shear forces and, thus, upward flow is significantly influenced by inclination.

6.2. Uncertainty analysis

As mentioned, a large number of heat transfer data point conditions for the microfin and the smooth tubes are presented in this paper (see Table 2). An uncertainty analysis was done for the heat transfer coefficient as described by Moffat [92].

6.2.1. Heat transfer coefficients

For the smooth tube, the uncertainties of the average heat transfer coefficient varied between 0.8% and 13.3%. Generally, higher values of uncertainties were obtained during downward flow. The lowest uncertainty occurred when the mass flux was 300 kg/m^{2}s, when the vapour quality was 25% and when the inclination angle was -30°. The largest uncertainty occurred for a mass flux of 400 kg/m^{2}s, a vapour quality of 90% and an inclination angle of -5°.

On the contrary, for the microfin tube, the largest uncertainties were obtained during the upward flow, particularly at inclination angles of +30° and +60°. The range of uncertainties was between 1.0% and 17.5%. The lowest uncertainty was obtained when the mass flux was 200 kg/m^{2}s for mean vapour quality of 25% and an inclination angle of -5°. The highest uncertainty occurred when the mass flux was 600 kg/m^{2}s for a vapour quality of 50% and an inclination angle of +30°. The greatest contribution to the uncertainties resulted from the measurement errors of the wall temperatures.

6.2.2. Pressure drop

An uncertainty analysis was done for the measured pressure difference as described by Moffat [92]. The uncertainties of the measured pressure difference varied between 0.05 kPa and 0.17 kPa. The highest uncertainty was obtained for a mass flux of 300 kg/m^{2}s, quality of 10% and an inclination

angle of +60°. At this condition, the uncertainty was 1.79%; however, most of the uncertainties were less than 0.07 kPa for most of the other measuring points in the test matrix.

6.3. Flow patterns for microfin tube

Fig. 7 presents the observed types of flow patterns encountered during the experiments. They include stratified-wavy (SW), annular-wavy (AW), annular (A), intermittent (I) and churn flow (C) flow patterns. For the operating conditions used in this investigation, the microfin tube did not exhibit any new type of flow pattern different from those observed for the smooth tube. However, it was observed that the flows tend to be more annular due to the turbulence introduced by the fin effect.

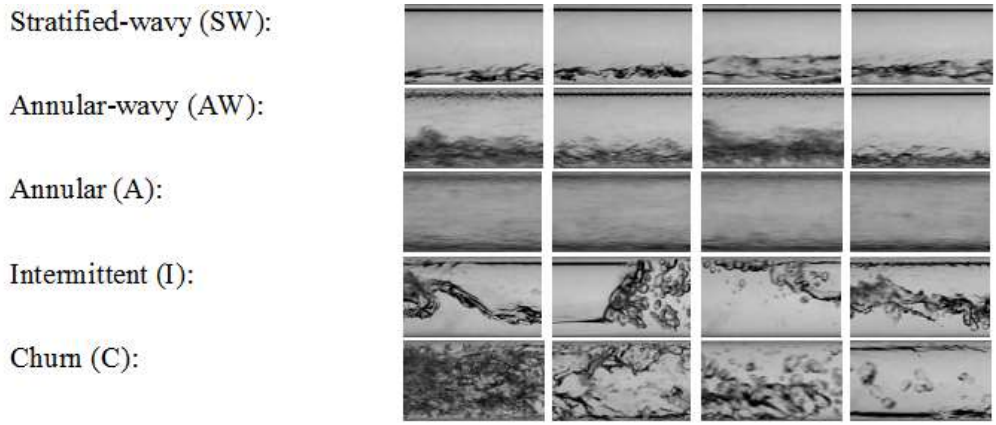

Fig. 7. The different types of flow patterns observed in this study and the terminology used for flow patterns described as stratified-wavy, annular-wavy, annular, intermittent and churn flow.

Fig. 8 reveals the variation of the flow pattern in the microfin tube with respect to the mean vapour quality and inclination angle at a mass flux of 300 kg/m^{2}s.

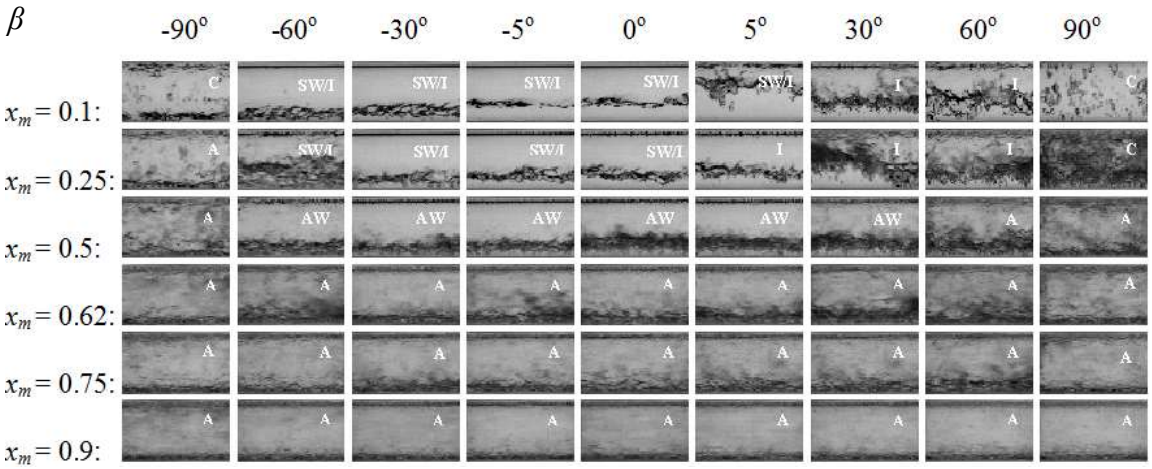

Fig. 8. Effect of inclination angle on the flow pattern in the microfin tube for different mean vapour qualities for a mass flux of 300 kg/m^{2}s.

In terms of the inclination angle from vertical downward flow to vertical upward flow, the following can be noted: For a mean vapour quality of 10%, the flow pattern was churn flow at β = -90°, it switched to stratified-wavy-intermittent flow as observed between β = -60° and +5°, it switched to intermittent flow as observed from β = 30° to 60°, and reverted back to churn flow as observed at β = +90°. A similar progression was observed for a mean vapour quality of 25%, except that instead of churn flow at β = -90°, annular flow was present, and the switch to "pure" intermittent flow was visible at β = +5° instead of at +30°. For a mean vapour quality of 50%, churn flow, stratified-wavy flow and intermittent flow were not observed. Instead, the flow changed from annular flow at β = -90° to annular-wavy flow as was visible between β = -60° and +30°, and back to annular flow as was visible between β = +60° and +90°. For mean vapour qualities of 62%, 75% and 90%, only annular flow was observed irrespective of the inclination angle.

Fig. 9 shows the variation of the flow pattern in terms of the inclination angle and the mass flux at a mean vapour quality of 50%. At a mass flux of 100 kg/m^{2}s, churn flow was observed at β = -90°, stratified-wavy flow was observed from β = -60° to 0°, stratified-wavy-intermittent flow was present at β = +30°, followed by intermittent flow observations at β = +30° and 60° and churn flow at β = +90°. For a mass flux of 200 kg/m^{2}s, almost the same flow patterns were identified. For 300 kg/m^{2}s,

only annular flow and annular-wavy flow were present, while for 400 and 600 kg/m^{2}s, annular flow was present irrespective of the inclination angle.

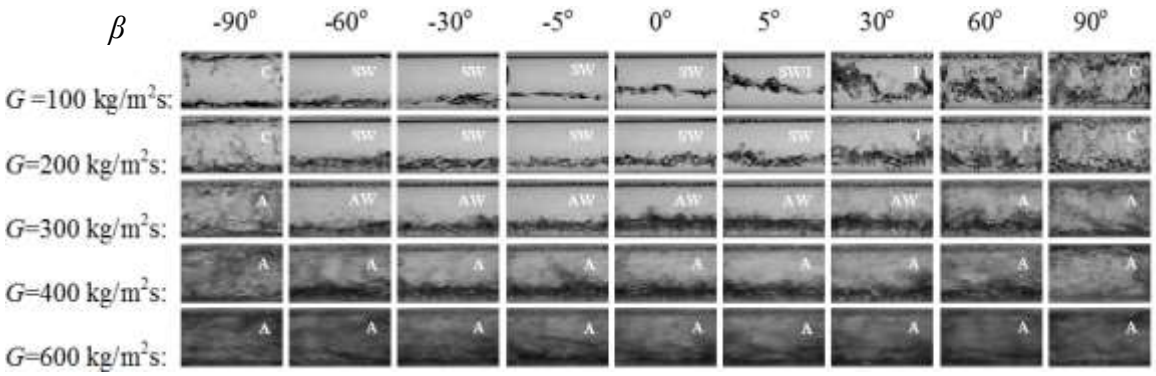

Fig. 9. Effect of the inclination angle on the flow pattern in the microfin tube for different mass fluxes for a quality of 50%.

6.4. Heat transfer coefficients

Results obtained for the smooth tubes were presented in earlier publications [10-12, 43, 44] using the same experimental facility, operational conditions and procedures. Interested readers are invited to consult these articles for an in-depth discussion of results. In this paper, new experimental data are presented for the microfin tube only. However, these results are compared with those of the smooth tube in a later section of this article.

In this section, the effects of the mean vapour quality, the mass flux and the inclination angle are investigated on the heat transfer coefficient in the microfin tube. An overview of the results shows that these parameters strongly influence the heat transfer coefficient in this type of tube, similar to the case with smooth tubes as reported by [7-10].

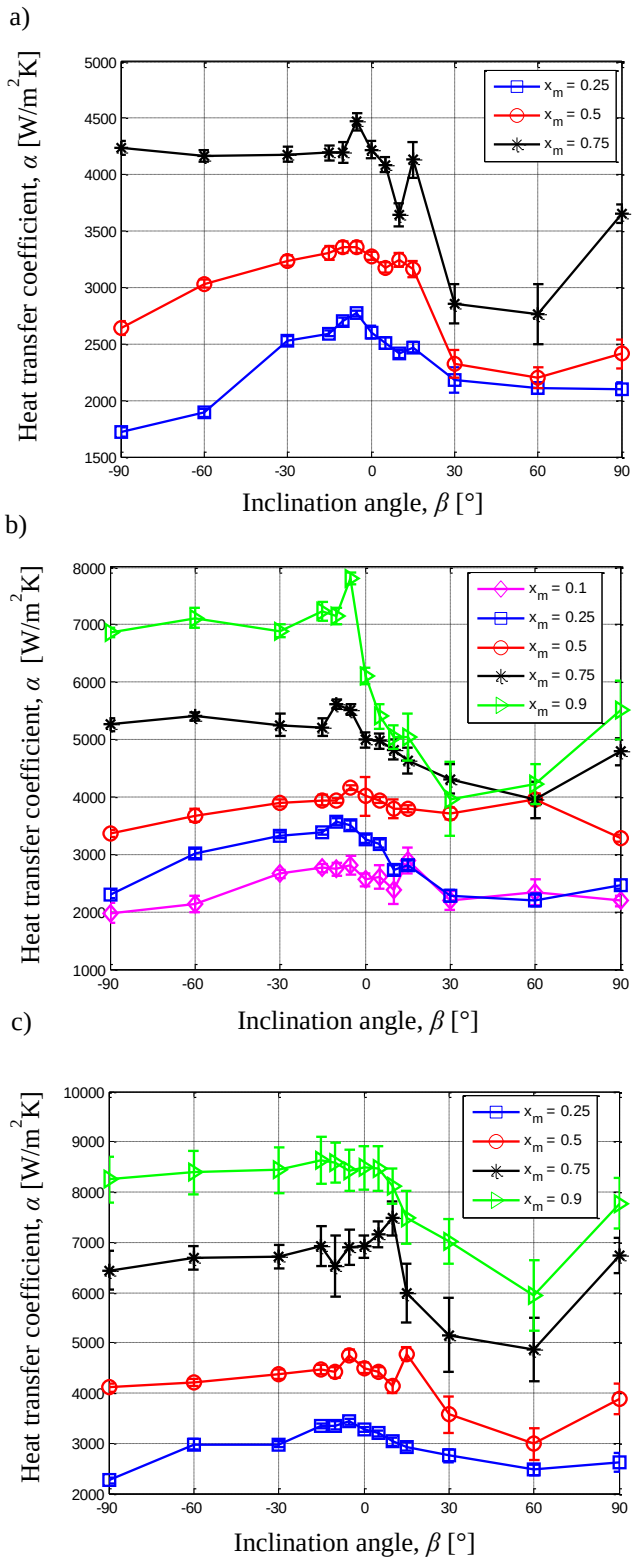

Fig. 10. Effect of inclination angle on heat transfer coefficient in the microfin tube for different vapour qualities for mass fluxes of a) 200 kg/m^{2}s, b) 300 kg/m^{2}s and c) 400 kg/m^{2}s.

Consider Figs. 10a-c, which show the heat transfer coefficients on the vertical axes in terms of the inclination angle on the horizontal axes at different mass fluxes and vapour qualities. In general, heat transfer coefficients increase with vapour quality and mass flux. The effect of inclination angle is equally important when comparing the upward and downward flow profiles. During the downward flow ($-90^o \leq \beta < 0^o$), increases in the vapour quality and the mass flux tend to reduce the effect of inclination on the flow. It can also be noted that there is a sudden reduction in the heat transfer coefficient between inclination angles of -5° and +30° or +60°, especially for a vapour quality of 90%. The effect of the inclination is thus more pronounced during upward flow, particularly as vapour quality increases because the film becomes thicker and the fins are submerged under the condensate thus reducing the surface tension effect.

Fig. 10 also indicates that there is a reversal of trends during both tube orientations (i.e. upward and downward tube orientations). There is a slight increase in the heat transfer coefficient from vertical downward (β = -90°) to the highest value at inclination angle between -5° and -15° (downward flow), after which there is a reversal in the trend of the heat transfer coefficient as the tube is oriented upwards. The effect of inclination during the downward flow can be seen most clearly for mean vapour quality between 10% and 50%, while it is insignificant for higher vapour qualities. At an inclination angle of +30° and +60° (upward flow), the lowest heat transfer coefficients were recorded due to the increasing liquid holdup (hence thermal resistance) in the flow for all the vapour qualities (except for a few cases, i.e. vapour quality of 10% for mass flux of 200 kg/m^{2}s, vapour qualities of 10% and 50 % for mass flux of 300 kg/m^{2}s and vapour qualities of 25% and 75% for mass flux of 400 kg/m^{2}s).

Figs. 11a-c present the same heat transfer coefficient data as in Fig. 10, but plotted with the vapour quality on the horizontal axes. It is shown that the heat transfer coefficient increases with quality, but not uniformly. It can be seen that the highest heat transfer coefficients are consistently obtained at an inclination angle of -5° (black dashed line), or in a few cases, at an inclination angle of +10°. The

lowest heat transfer coefficient occurs mostly at an inclination angle of +60°, or in a few cases, at inclination angles of -90°, +90° or +30°.

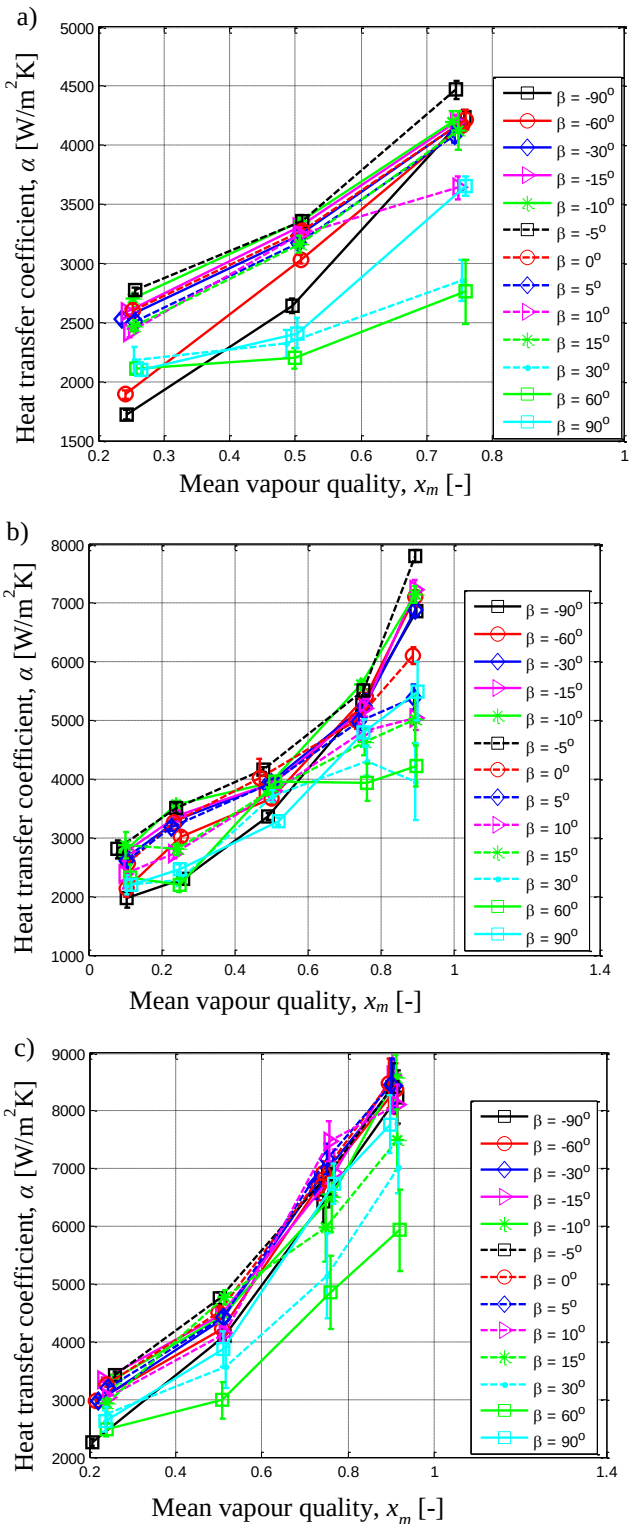

Fig. 11. Effect of mean vapour quality on heat transfer coefficient in the microfin tube for different inclination angles for mass fluxes of a) 200 kg/m^{2}s, b) 300 kg/m^{2}s and c) 400 kg/m^{2}s.

In order to better visualise the impact of the mass flux, the same data as in Figs. 10 and 11 are represented in Figs. 12 and 13 at different vapour qualities. Figs. 12 and 13 are plotted with horizontal axes showing the inclination angle and the mass flux respectively. For low vapour quality, Fig. 12a reveals that irrespective of the mass flux and orientation, the flows (whether downward or upward) are subject to the influence of inclination due to the influence of gravity forces on the liquid condensate. As the vapour quality increases, the downward flow seems to be less influenced (Figs. 12b-c) due to shear and fin effect, among others. Fig. 13a shows that for a vapour quality of 25%, the heat transfer coefficient does not necessarily increase with an increase in the mass flux. While there is an increase in the heat transfer coefficient with an increase in the mass flux between 200 kg/m^{2}s and 300 kg/m^{2}s irrespective of the inclination, it increases, decreases or remains the same between 300 kg/m^{2}s and 400 kg/m^{2}s. For a 50% vapour quality (Figs. 12b and 13b), only data for inclination angles of +30^o and +60^o appear to behave erratically as the mass flux increases. However, for a mean vapour quality of 75% (Figs. 12c and 13c), there is a corresponding increase in heat transfer coefficient with an increased mass flux, irrespective of the tube orientation.

This behaviour can be attributed to the fact that as vapour quality increases, the condensate film thickness decreases. During downward flow, due to the action of gravity in the same direction with the flow, there is the tendency of the condensate film to become slightly thinner, thus the fins are exposed to direct contact with the vapour increasing the heat transfer coefficient [20]. Moreover, a decrease of liquid film thickness promotes surface drainage between the fins. During upward flow, due to the action of gravity in the opposing direction to the flow and the slowdown in the vapour and liquid velocities, the condensate becomes thicker and promotes flooding towards the exit, hence the fin effect is reduced. Increase in the film thickness introduces thermal resistance during upward flow, hence the result is lower heat transfer coefficients.

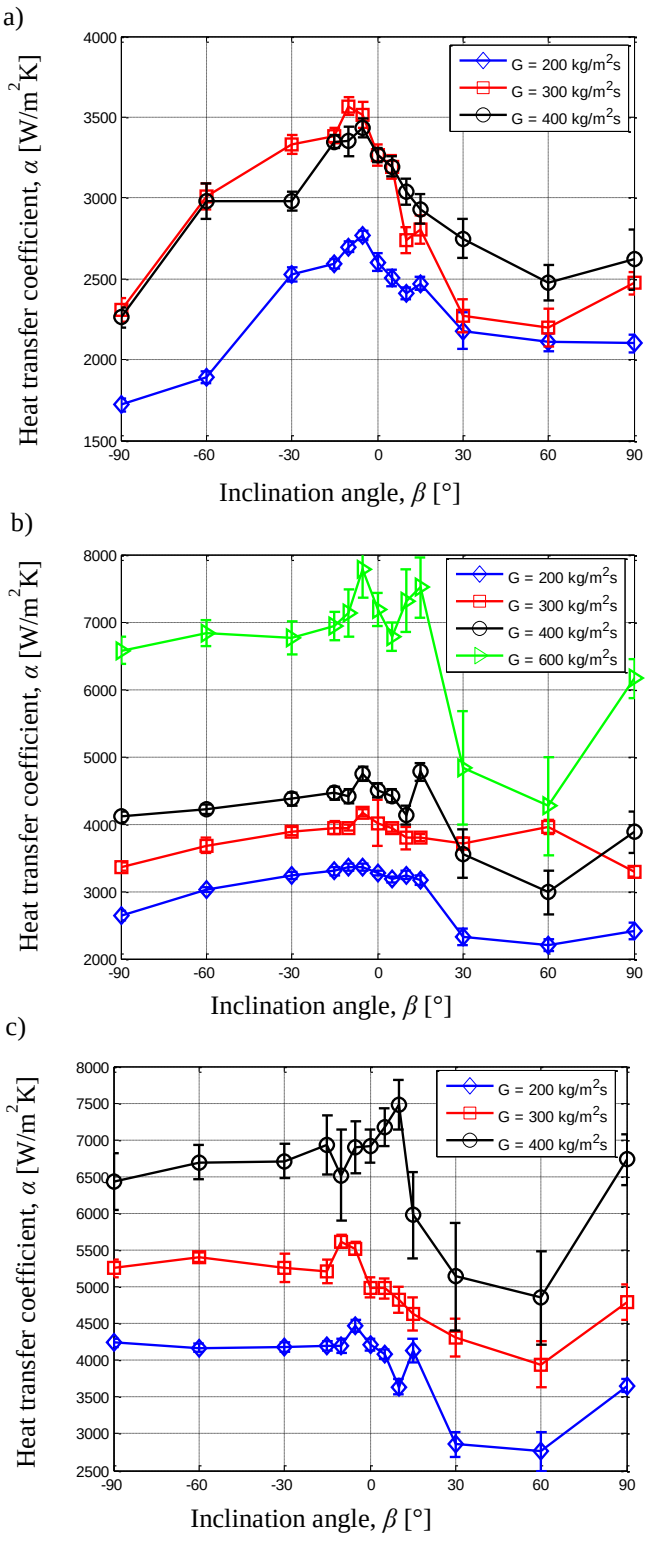

Fig. 12. Effect of inclination angle on heat transfer coefficient in the microfin tube for different mass fluxes for mean vapour qualities of a) 25%, b) 50% and c) 75%.

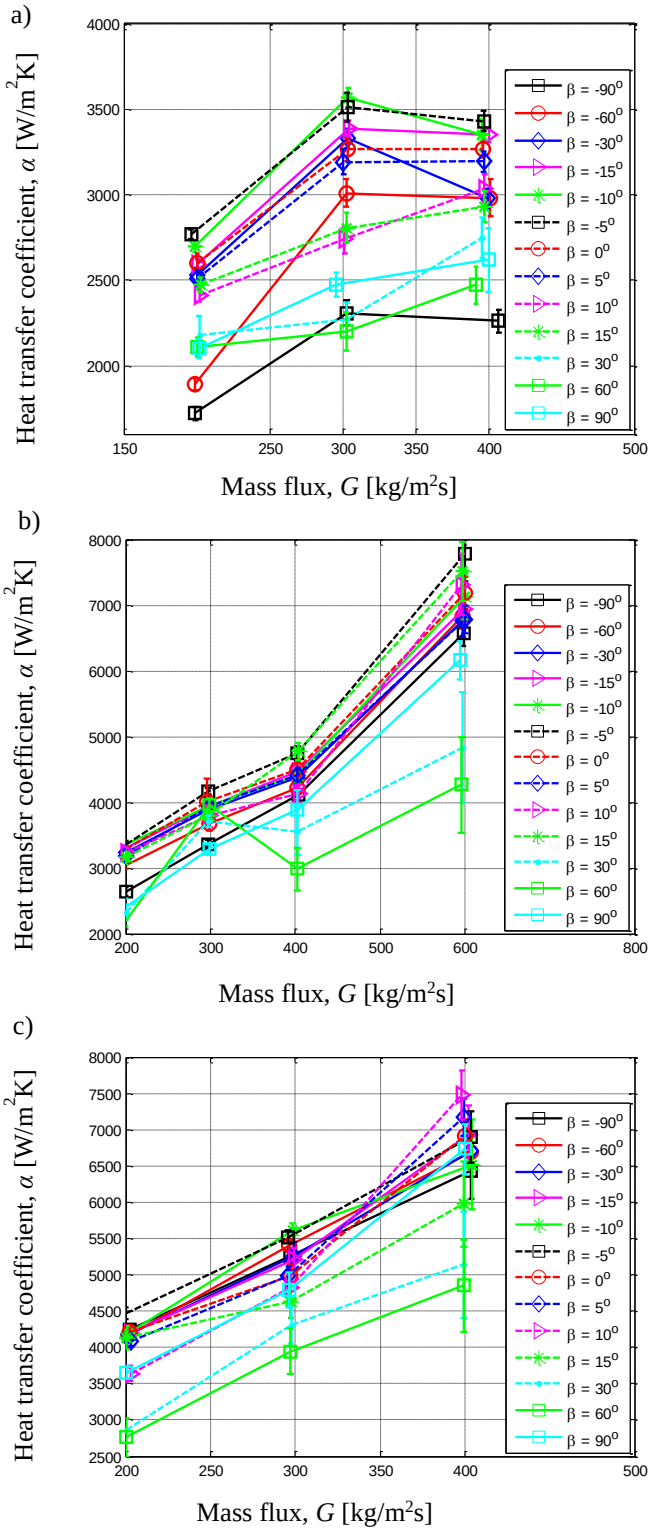

Fig. 13. Effect of varying mass fluxes on the heat transfer coefficient in the microfin tube for different inclination angles for mean vapour qualities of a) 25%, b) 50% and c) 75%.

6.5. Pressure drops in microfin tube

Fig. 14 gives the results of the variation of the measured pressure drops in the microfin tube in terms of the inclination angle and the mean vapour quality for mass fluxes of a) 200 kg/m^{2}s b) 300 kg/m^{2}s and c) 400 kg/m^{2}s. The general trend shows higher measured pressure differences during the upward tube orientation compared with during the downward orientation, except for cases with a vapour quality of 90% and for a mass flux of 300 kg/m^{2}s. This general trend is expected due to the influence of the static pressure difference. As the mean vapour quality increases, the measured pressure difference also increases for inclination angles between -90° and +15° for a mass flux of 200 kg/m^{2}s and between -90° and +30° for a mass flux of 300 kg/m^{2}s. For a mass flux of 400 kg/m^{2}s, the measured pressure differences were similar for vapour qualities of 75% and 90% between inclination angles of -15° and +5°. For inclination angles lower than -15°, the pressure differences for a mean vapour quality of 90% are slightly higher, while beyond, the pressure differences for a mean vapour quality of 75% are higher. In all other cases, the measured pressure differences increase with vapour quality irrespective of the inclination angle. Due to the predomination of the frictional pressure difference resulting in higher shear force as vapour quality increases, the effect of static pressure hence, the inclination angle decreases for mass flux of 400 kg/m^{2}s.

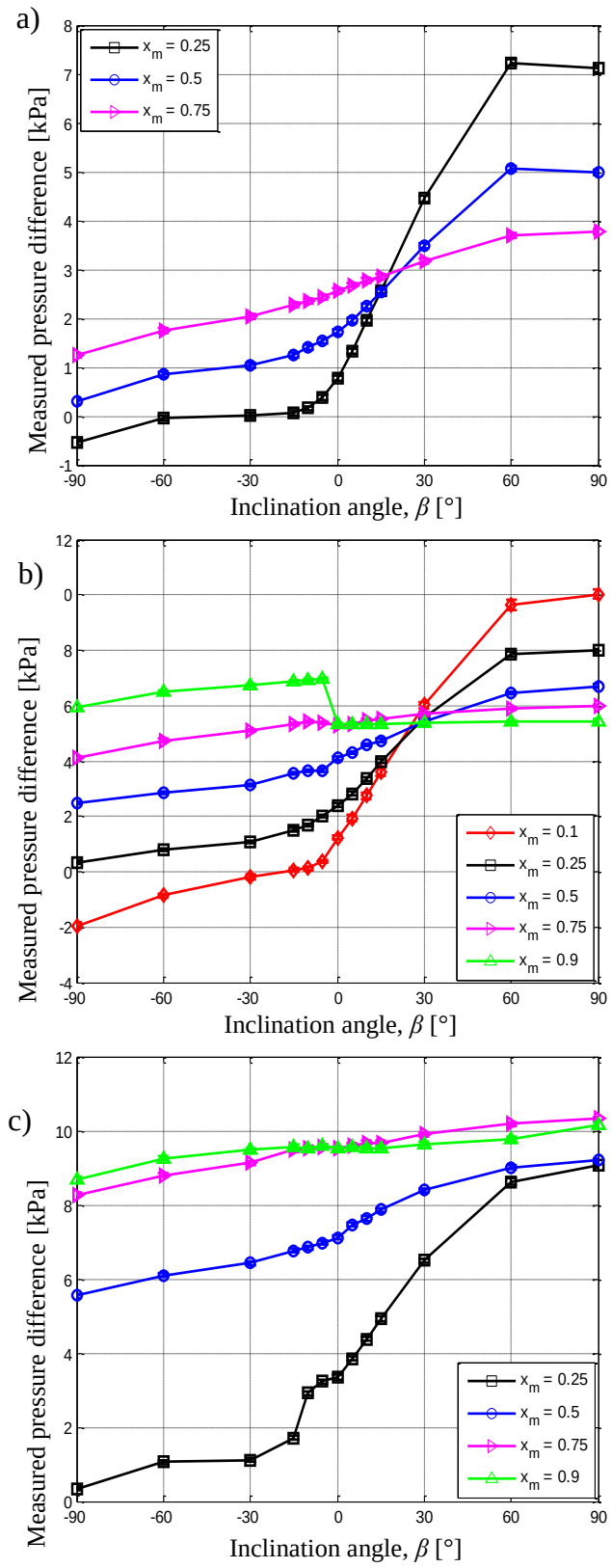

Fig. 14. Effect of inclination angle on the measured pressure difference in the microfin tube for different vapour qualities for mass fluxes of a) 200 kg/m^{2}s, b) 300 kg/m^{2}s and c) 400 kg/m^{2}s.

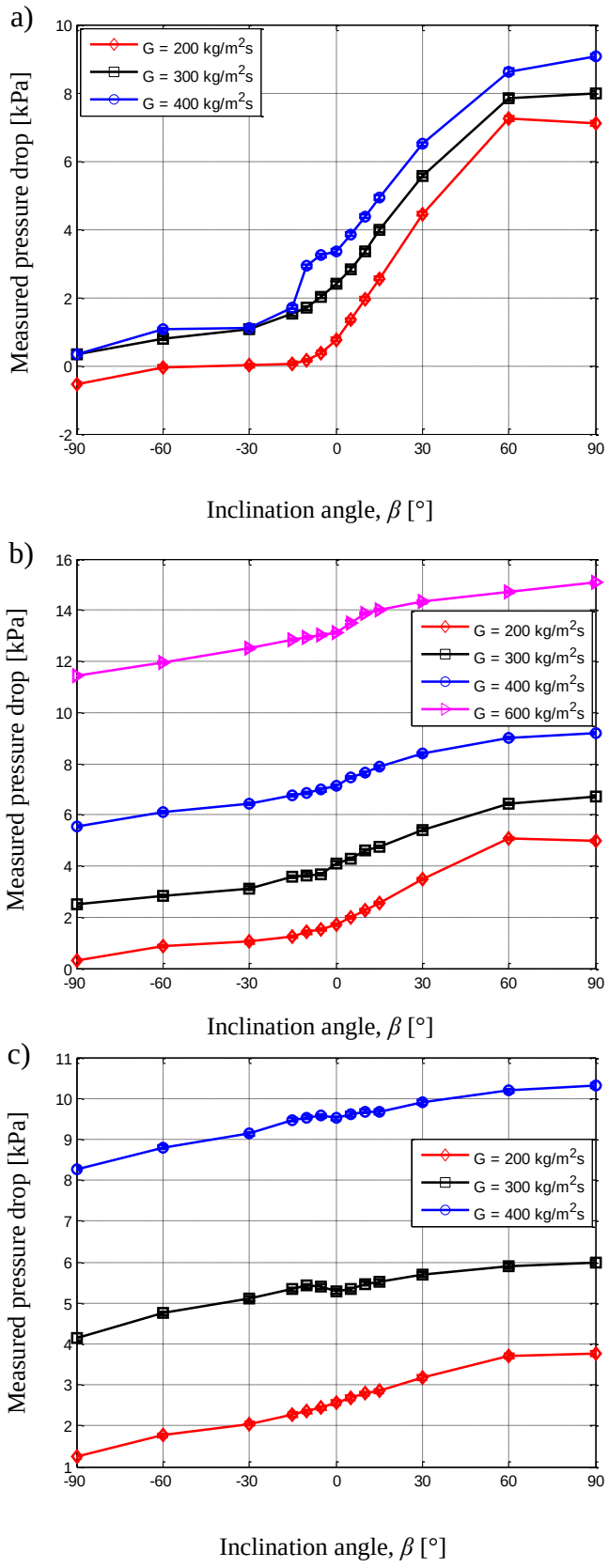

Fig. 15. Effect of inclination angle on the measured pressure difference in the microfin tube for different mass fluxes for vapour qualities of a) 25%, b) 50% and c) 75%.

Fig. 15 represents the measured pressure differences as a function of the inclination angle for different mass fluxes for mean vapour qualities of a) 25%, b) 50% and c) 75%. The results show that the measured pressure differences generally increase with mass flux and vapour quality. With inclination angle, the pressure differences monotonically increase as β increases from -90° to +90°. As β increases, the liquid holdup increases due to the static pressure difference. Also, as quality increases, the measured pressure differences increase. This is due to increases in the frictional pressure drop resulting from the shear effects and the static pressure drop decreases resulting from a decrease in the liquid holdup.

6.5.1. Predicted void fraction

Fig. 16 reveals the variation of the calculated void fraction using the model in terms of the inclination angle for mean vapour qualities between 10% and 90% for mass fluxes of a) 200 kg/m^{2}s b) 300 kg/m^{2}s and c) 400 kg/m^{2}s. It is shown that an increase in the mean vapour quality gives a corresponding increase in the void fraction. It is also shown that the inclination angle does not have a large impact on the calculated void fraction. However, for mass fluxes of 200 kg/m^{2}s and 300 kg/m^{2}s, higher void fraction values are obtained during the downward flow than during the upward flow. This could possibly be because the model takes into consideration that during downward flow, due to the action of the gravitational force in the direction of flow, the condensate film becomes thinner thus increasing the void fraction. On the other hand, during upward flow, the condensate becomes thicker reducing the void fraction. For a mass flux of 400 kg/m^{2}s, this is not the case as the effect of gravitational force seems reduced because the shear force is stronger.

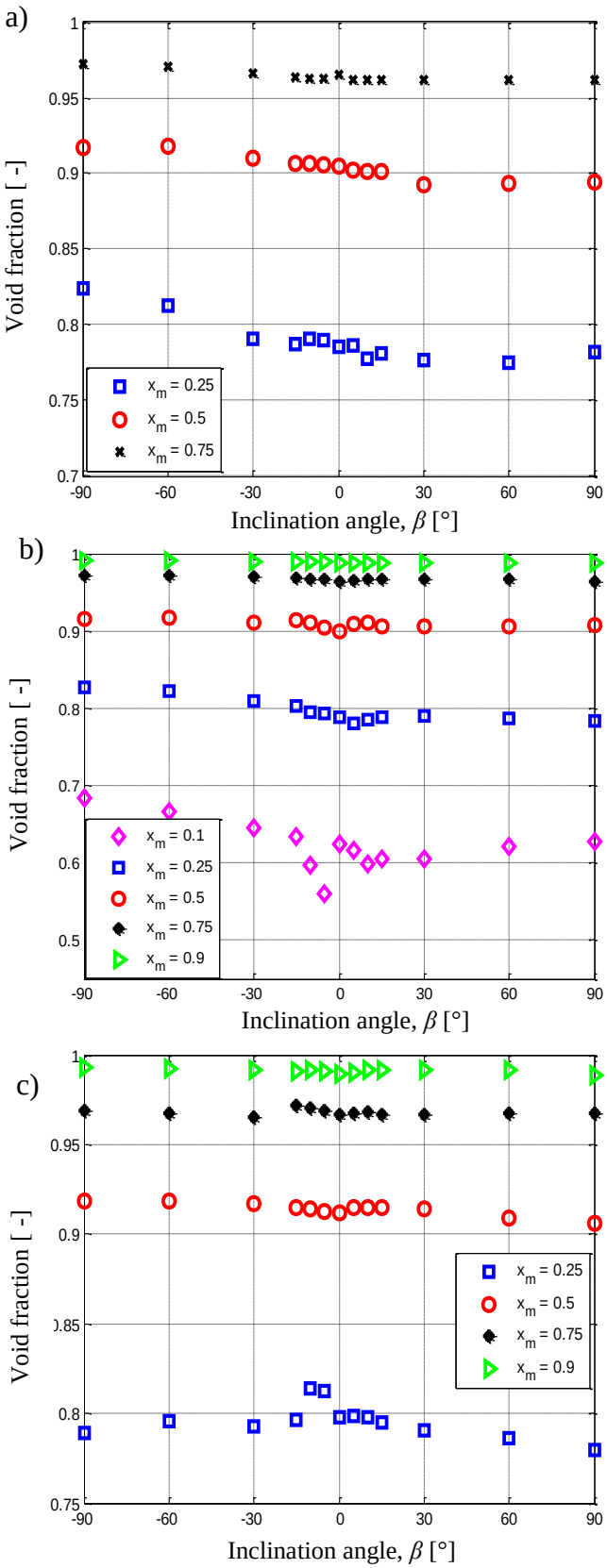

Fig. 16. Effect of inclination angle on void fraction in the microfin tube for different vapour qualities for mass fluxes of a) 200 kg/m^{2}s, b) 300 kg/m^{2}s and c) 400 kg/m^{2}s.

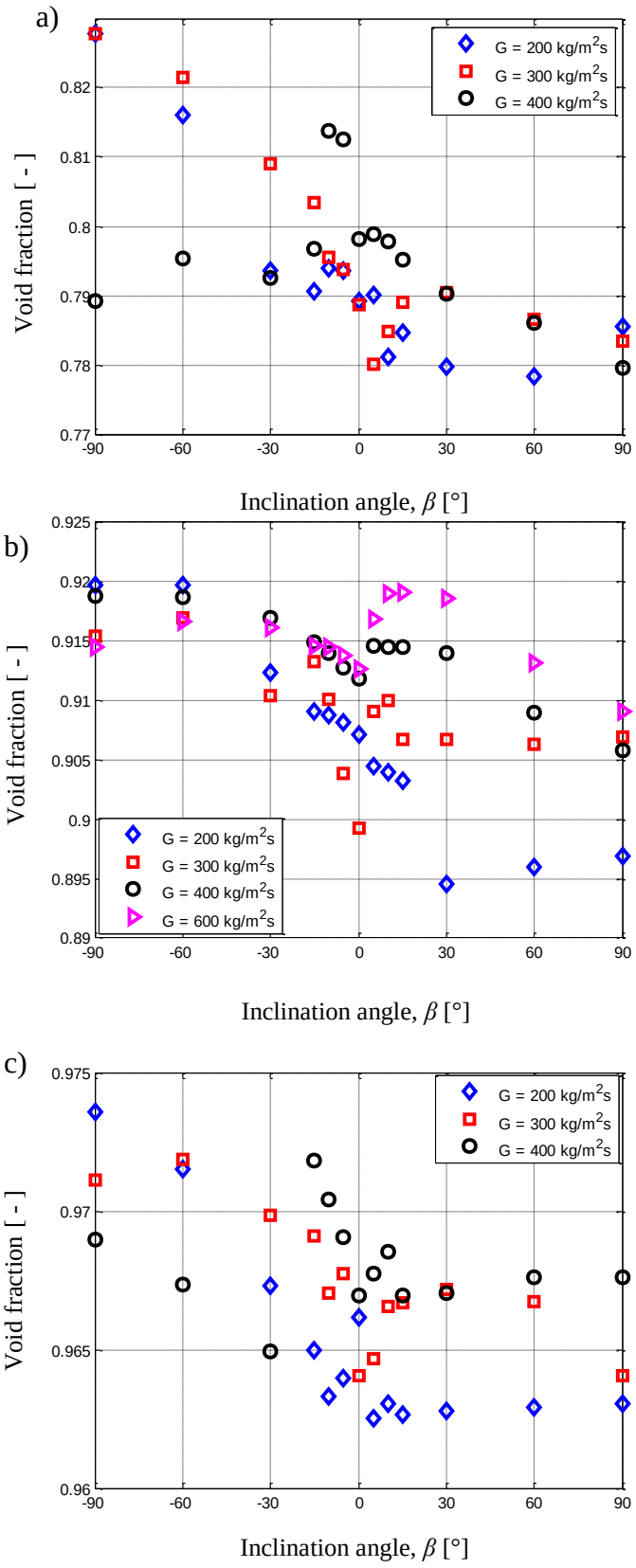

Fig. 17. Effect of inclination angle on void fraction in the microfin tube for different mass fluxes for vapour qualities of a) 25%, b) 50% and c) 75%.

Fig. 17 represents the same data but by showing the effect of inclination angle and mass flux on the void fraction while maintaining a constant mean vapour quality of a) 25%, b) 50% and c) 75%. Except for the vertical upward tube orientation, during the inclined upward flow, the void fraction seems to respond positively as it largely increases with high mass flux in this region.

6.5.2. Frictional pressure drop

The results of the frictional pressure drop as it varies with inclination angle, mean vapour quality and mass flux are presented in Figs. 18 and 19. Shown in Fig. 18 are results for the effect of the mean vapour qualities on frictional pressure drops for mass fluxes of a) 200 kg/m^{2}s, b) 300 kg/m^{2}s and c) 400 kg/m^{2}s, while Fig. 19 shows the effect of the mass flux at selected constant mean vapour qualities of a) 25%, b) 50% and c) 75%. There is an overall increase in the frictional pressure drop with quality and mass flux. By closely observing, for example, the profile of the frictional pressure drop for a mass flux of 200 kg/m^{2}s to 300 kg/m^{2}s and quality of less than 50% (Figs. 18a, b, 19a), and matching it with the flow pattern profiles in Figs. 8 and 9, the conspicuous turning points during the inclination of -60° and +60° can be attributed to the change in flow pattern with inclination angle. The points of inflexion are thus the transition points between flow regimes such that there is a churn to stratified-wavy flow transition (at β = -60°), stratified-wavy to intermittent flow transition (at around β = 0°) and intermittent to churn flow transition (at β = +60°). The increase in the pressure drop during the upward flow is a result of the higher liquid holdup. For higher mean vapour qualities equal to or greater than 75% for mass fluxes of 200 kg/m^{2}s and greater (Figs. 18a, 19c) and equal to or greater than 50% for mass fluxes of 300 kg/m^{2}s and 400 kg/m^{2}s (Figs. 18b, c, 19b, c), frictional pressure drop monotonically decreases with inclination angle between -60^o and +90^o as a result of decrease in shear force.

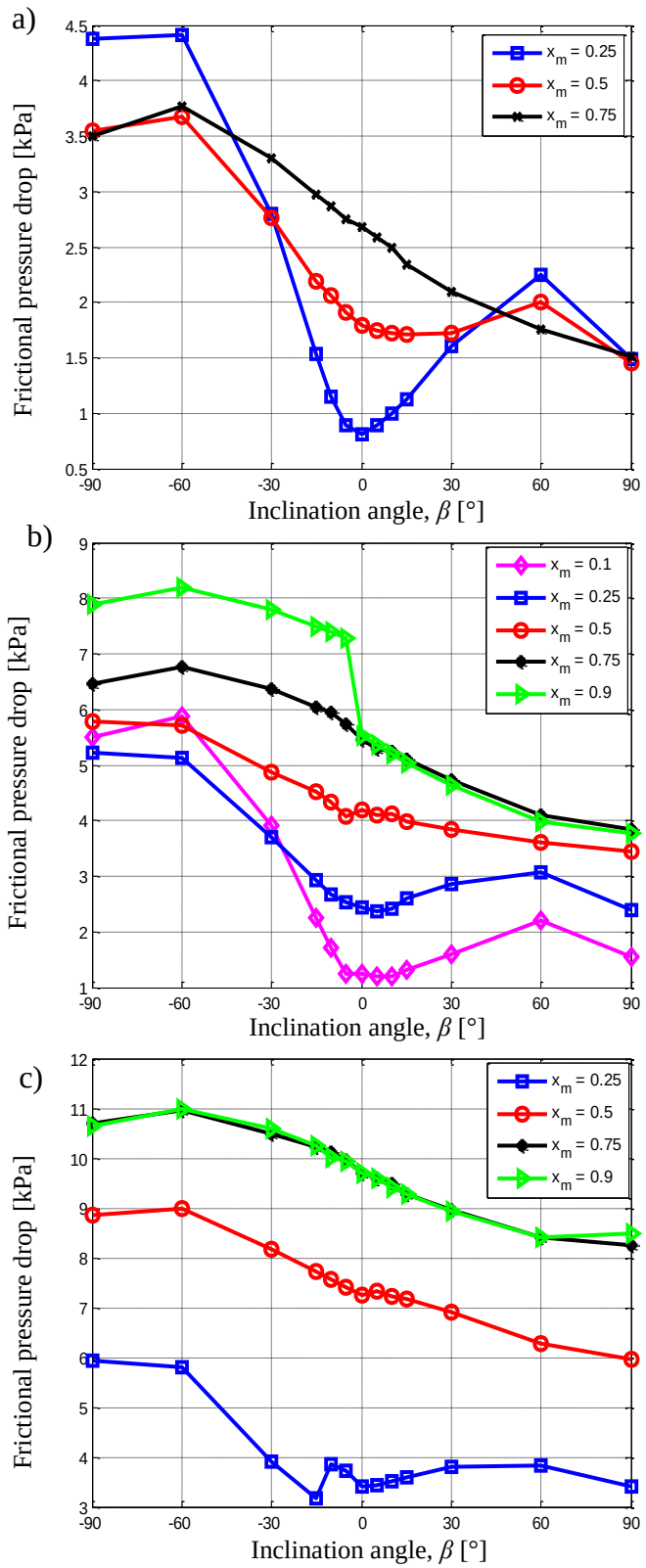

Fig. 18. Effect of inclination angle on frictional pressure drop in the microfin tube for different vapour qualities for mass fluxes of a) 200 kg/m^{2}s, b) 300 kg/m^{2}s and c) 400 kg/m^{2}s.

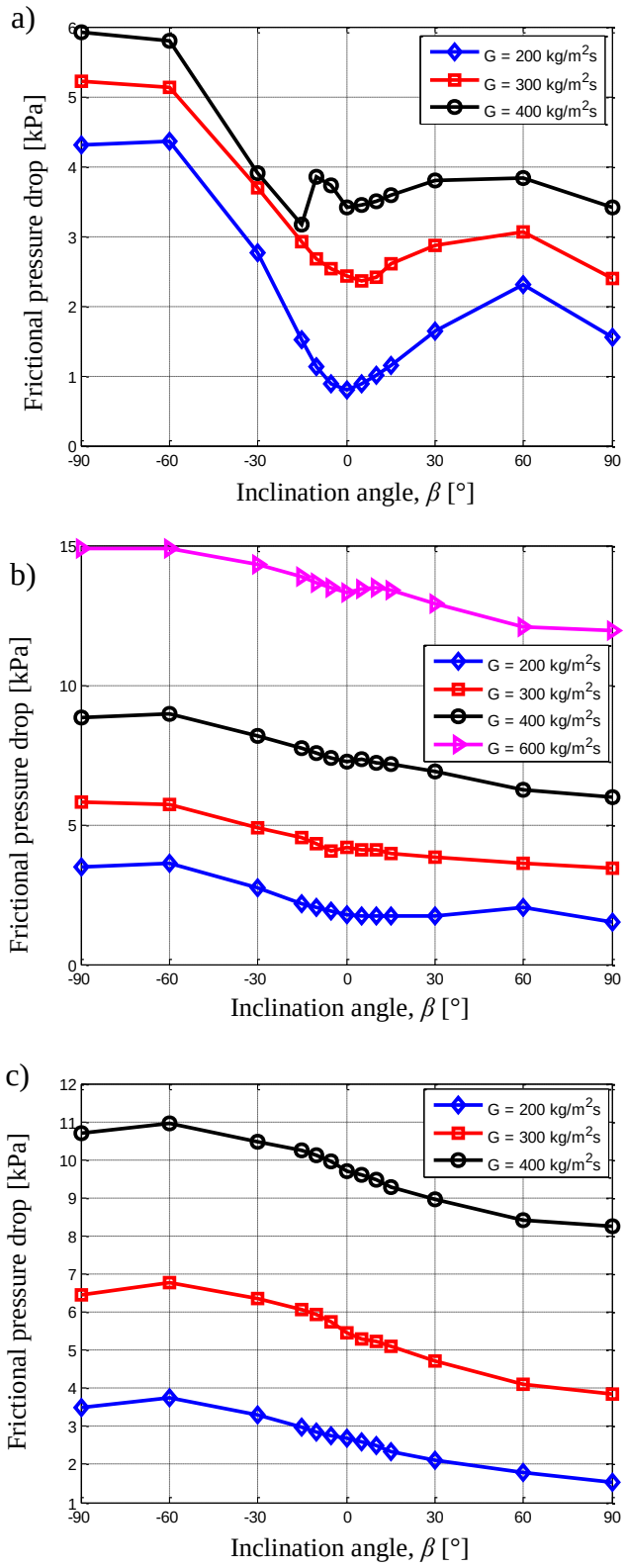

Fig. 19. Effect of inclination angle on frictional pressure drop in the microfin tube for different mass fluxes for vapour qualities of a) 25%, b) 50% and c) 75%.

6.6. Comparison with smooth tube results

6.6.1. Enhancement factor

The enhancement factor (*EF*), defined as the ratio of the heat transfer coefficients obtained with the microfin tube to that of the smooth tube, is a useful measure of comparison. Subject to the same operating conditions, this is expressed as follows:

$$EF = \frac{\alpha_{microfin}}{\alpha_{smooth}} \tag{12}$$

where $\alpha_{microfin}$ is the heat transfer coefficient of the microfin tube and α_{smooth} is the heat transfer coefficient of the smooth tube.

Due to the larger inner heat transfer surface of the finned tube compared with that of the smooth tube, the surface area ratio also needs to be determined in order to make more substantial comparisons between the heat transfer coefficients obtained with the different tube types. The actual heat transfer surface area of the finned tube can be calculated in terms of the number of fins, *N*, the fin height, *e*, and the helix angle, *H*, as follows, as given by Bukasa et al. [93]:

$$A_a = L_t\left(\pi d_i + \frac{2N.e}{\cos H}\right) \tag{13}$$

As mentioned, the smooth tube has an inner diameter of d_i = 8.38 mm. By using equation (13) to calculate the microfin actual heat transfer surface area and comparing it with the surface area of the smooth tube (A_a/A), the microfin-to-smooth tube area ratio is 2.05. This is important when considering the relative differences in the heat transfer results. For both smooth and microfin tubes, as quality increases, the thermal resistance reduces due to the reduction in the liquid film thickness whatever the inclination angle. Also, with increase in inclination angle, the flow opposes gravity and the velocity of the flow is slightly lowered leading to a thicker film, hence, reduced thermal resistance and reduced heat transfer coefficient.

Since microfin tubes have extended contact area, the heat transfer coefficient generally increases. There are additional forces that are introduced due to the presence of fins. These forces are associated with turbulence and surface tension.

As quality increases, the effect of the fin becomes more noticeable. At high quality, the fin can be exposed to the vapour during which the surface tension is very significant coupled with the reduced thermal resistance leads to increased heat transfer coefficient. However, as inclination angle increases towards the upward flow, the increased thickness covers the fin hence increasing the thermal resistance and reduced the surface tension. This undoubtedly reduces the heat transfer coefficient.

Figs. 20 a - c present the heat transfer coefficient results for both smooth and microfin tubes for mass fluxes of 200 kg/m^{2}s, 300 kg/m^{2}s and 400 kg/m^{2}s for different mean vapour qualities depending on available data. Microfin tube data are represented with solid lines and smooth tube data are represented with dashed lines. It is clearly shown that in general, the heat transfer coefficients for the microfin tube are significantly greater than those for the corresponding quality and mass flux in the smooth tube. With respect to the inclination angle, the highest heat transfer coefficients are found to be at inclination angles of either between -30° and -15° for the smooth tube, or between -15° and -5° for the microfin tube.

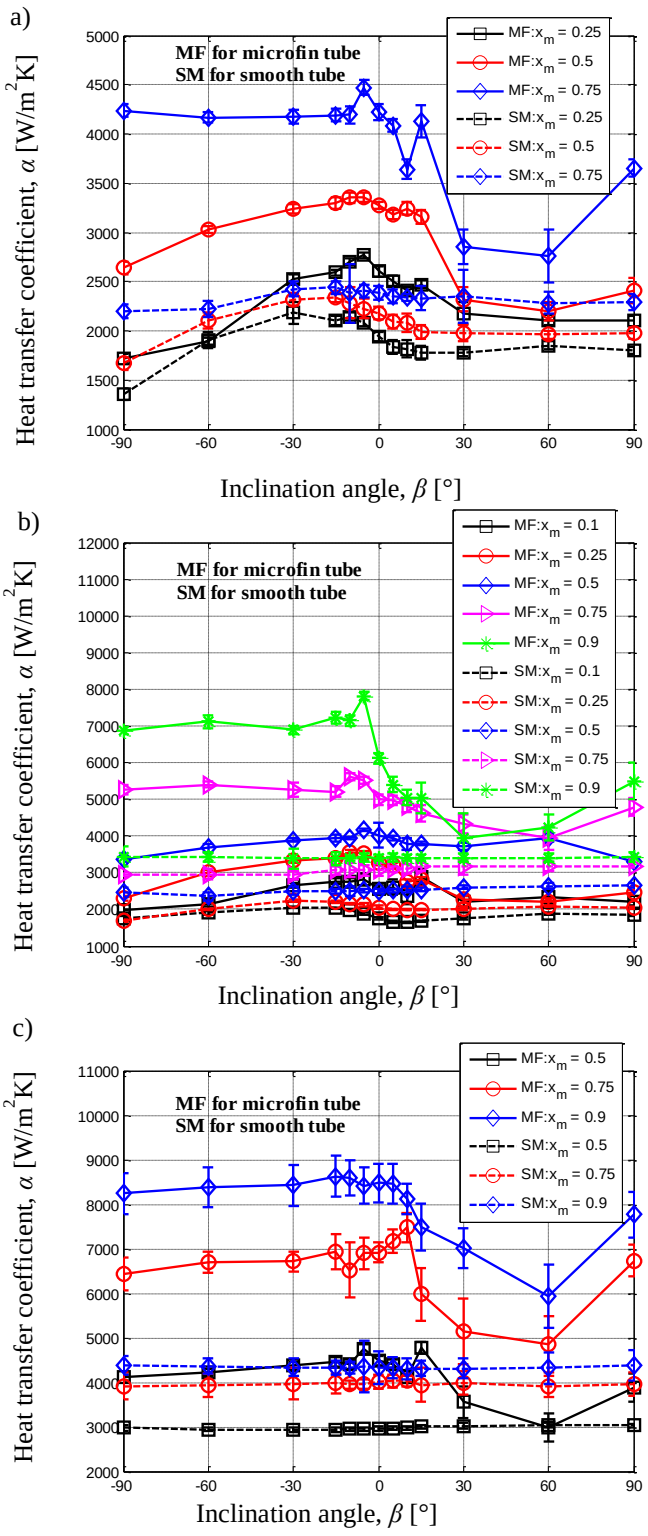

Fig. 20. Comparison between the heat transfer coefficient in microfin and smooth tubes for different qualities and inclination angles for mass fluxes of a) 200 kg/m^{2}s, b) 300 kg/m^{2}s and c) 400 kg/m^{2}s.

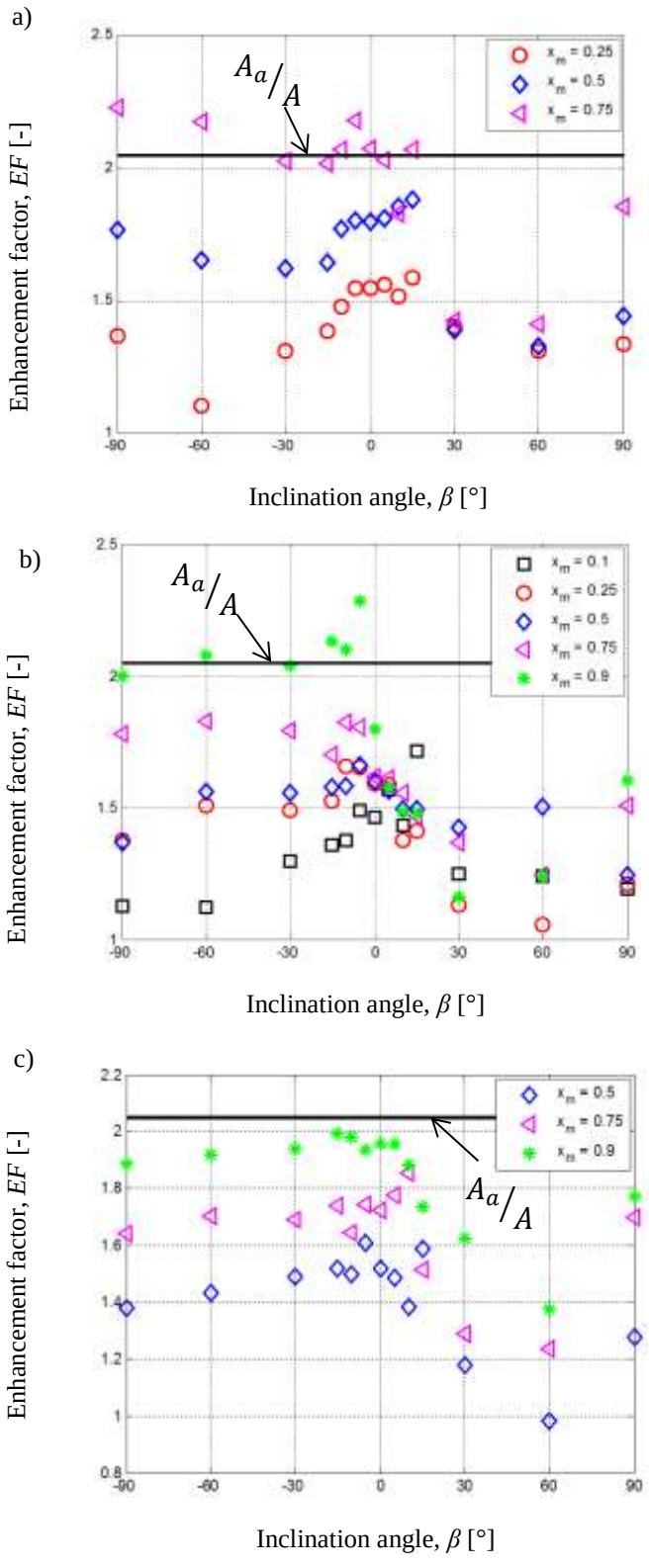

Fig. 21. Effect of inclination angle on the heat transfer enhancement factor for different vapour qualities for mass fluxes of a) 200 kg/m^{2}s, b) 300 kg/m^{2}s and c) 400 kg/m^{2}s.

Fig. 21 presents the heat transfer enhancement factors obtained from equation (12) based on the average heat transfer coefficients for the microfin tubes in comparison with those for the smooth tubes as they vary with quality, mass flux and inclination angle. The figure reveals the variation of the heat transfer enhancement with inclination angle for different vapour qualities. For convenience, the microfin-to-smooth tube surface area ratio of 2.05 is included in the figure by the solid line.

The variations of the enhancement factor with inclination angle for different vapour qualities for mass fluxes of 200 kg/m^{2}s, 300 kg/m^{2}s and 400 kg/m^{2}s are shown. The downward inclinations and horizontal flow orientation give higher enhancements compared with the upward flow inclinations for vapour qualities of 50% and greater.

This is because of higher local heat transfer coefficients in the microfin tube, as explained earlier. For most of the tube orientations, there is an increase in enhancement with quality. This is largely applicable to upward flow in the case shown in Fig. 21a and Fig. 21c, but not for a mass flux of 300 kg/m^{2}s as shown in Fig. 21b. The highest enhancement factor of 2.38 is obtained during downward flow for an inclination angle of -5° and mass flux of 300 kg/m^{2}s, while the lowest is 0.98, which is obtained during upward flow for an inclination angle of -60^o and mass flux of 400 kg/m^{2}s. Han and Lee [20] and Kedzierski and Goncalves [30] also reported a heat enhancement factor less than unity in their experiments. A closer look reveals that heat transfer enhancement increases with quality during downward flow and this is due to shear and fin effects. It is also important to note that for most of the test conditions, the enhancement factor is lower than the surface area ratio, as judged by the position of the solid line in Fig. 21. Conditions with a mass flux of 200 kg/m^{2}s (Fig. 21a) resulted in the most number of cases where the heat transfer coefficient enhancement factor was greater than the surface area ratio, followed by conditions with a mass flux of 300 kg/m^{2}s (Fig. 21b).

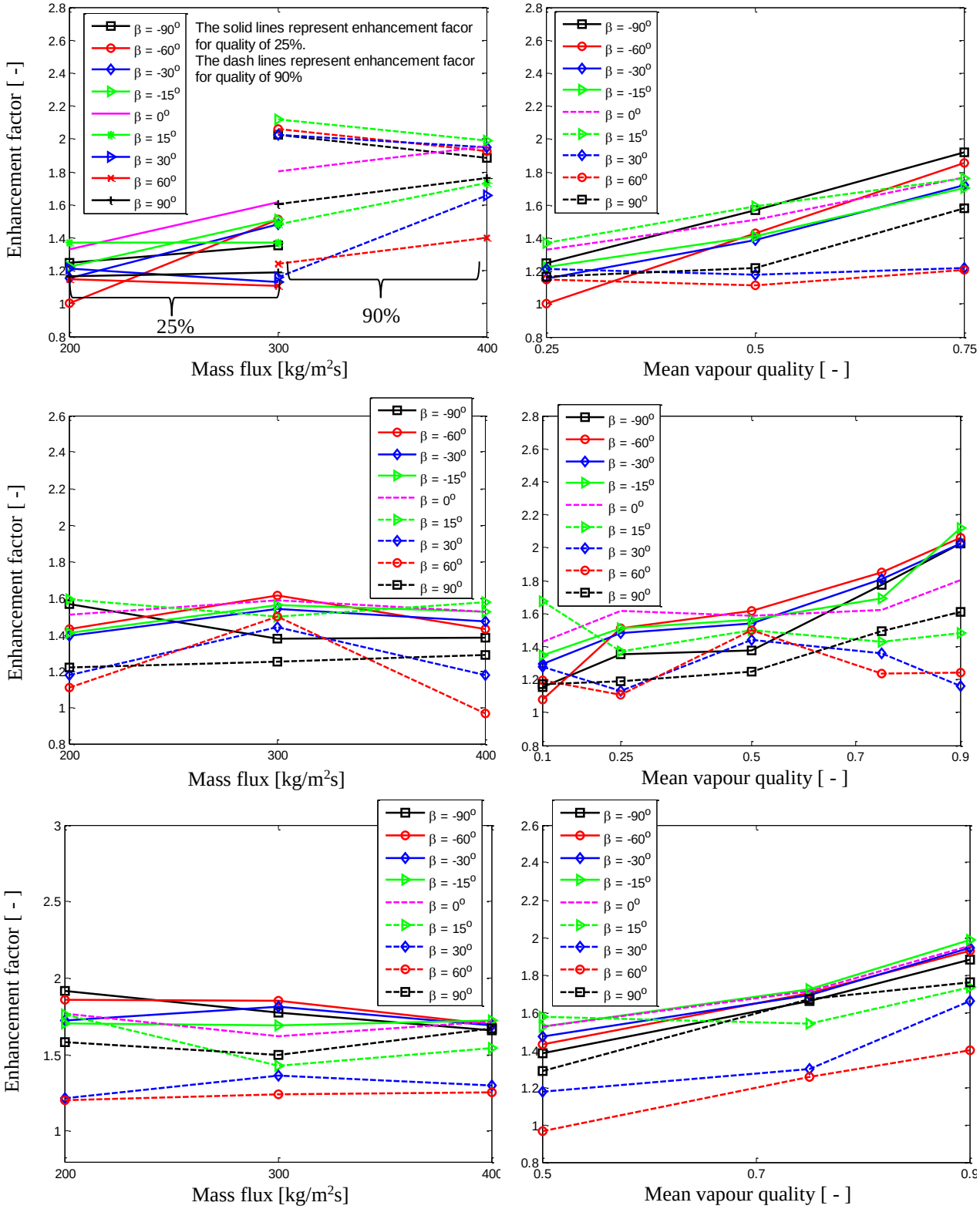

Fig. 22. Effect of mass flux on the heat transfer enhancement factor for different inclination angles for vapour qualities of a) 25% and 90%, b) 50% and c) 75%.

Fig. 23. Effect of mean vapour quality on the heat transfer enhancement factor for different inclination angles for mass fluxes of a) 200 kg/m^{2}s, b) 300 kg/m^{2}s and c) 400 kg/m^{2}s.

For conditions with a mass flux of 400 kg/m^{2}s (Fig. 21c), none of the cases resulted in an enhancement factor greater than the surface area ratio. Fig. 22 illustrates the relationship between the heat transfer enhancement factor and the mass flux for different inclination angles for mean vapour quality of a) 25% and 90%, b) 50% and c) 75%. It can be observed that for mean vapour quality of 25%, there was no reliable data for mass flux of 400 kg/m^{2}s, while for the vapour of 90%, there was no reliable data for mass flux of 200 kg/m^{2}s. This can be attributed to the fact that only data conditions available for both smooth and microfin tubes were used for the calculation of the enhancement factor and pressure penalty factor.

In this figure, enhancement can be said to have increased, decreased or remained constant with mass flux. On the other hand, no particular trend can be pinpointed based on the inclination angle as can be found in the open literature. Higher enhancements are observed during downward flow than during upward flow. Fig. 23 presents the enhancement factor as a function of the mean vapour quality for different inclination angles for mass flux of a) 200 kg/m^{2}s, b) 300 kg/m^{2}s and c) 400 kg/m^{2}s. A quick view shows that enhancement seems to have an increasing effect on the quality for most of the inclination angles.

6.6.2. Pressure penalty factor

As mentioned, the pressure penalty factor (PF) is defined as the ratio of the frictional pressure drop of the microfin tube to the frictional pressure of the smooth tube [20, 26].

$$PF = \frac{\Delta P_{fric,microfin}}{\Delta P_{fric,smooth}} \tag{14}$$

where $\Delta P_{fric,microfin}$ is the frictional pressure drop of the microfin tube and $\Delta P_{fric,smooth}$ is the frictional pressure drop of the smooth tube.

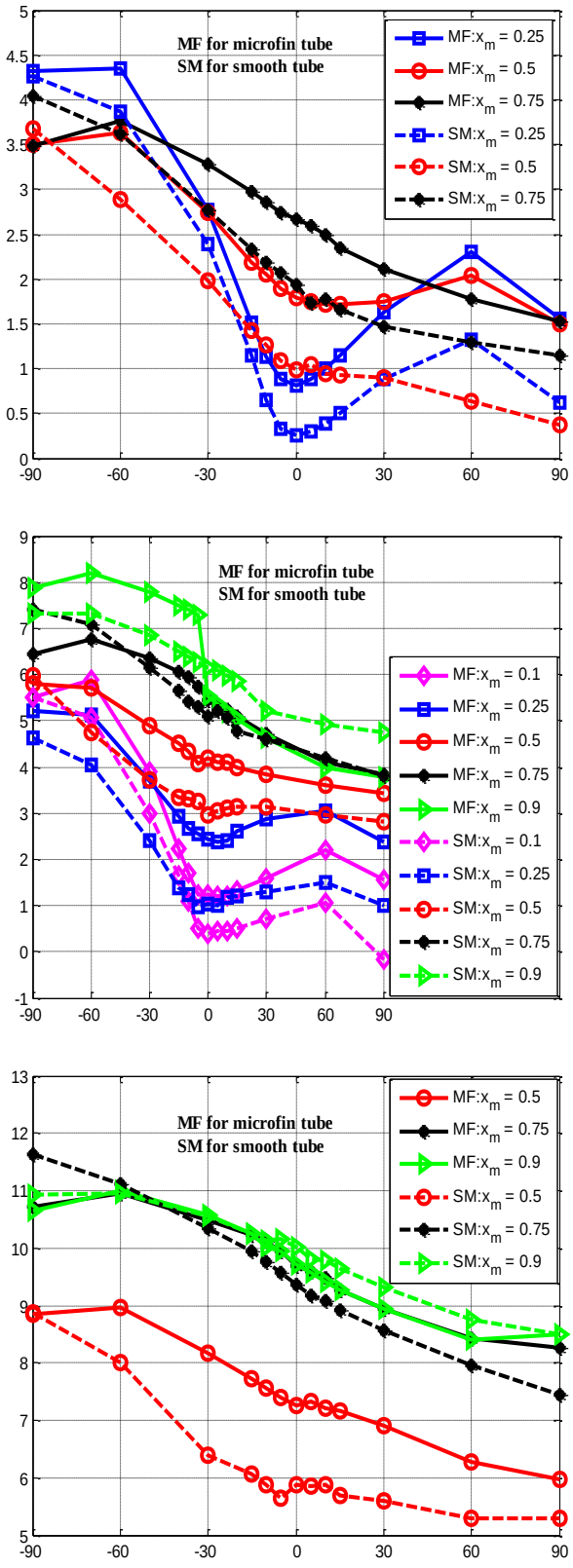

Fig. 24. Comparison between frictional pressure drop in microfin and smooth tubes for different mass fluxes for vapour qualities of a) 25%, b) 50% and c) 75%.

In order to clearly show how the pressure penalty factor is obtained, the frictional pressure drops of the smooth and the microfin tubes are plotted in Fig. 24 for mass flux of 200 kg/m^{2}s-400 kg/m^{2}s for the available vapour qualities for different inclination angles. Expectedly, the microfin tube gives a higher pressure drop for most of the data. This can be attributed to the turbulence and surface tension forces introduced by the presence of the fins [20, 91]. However, there are some exceptions in which the smooth tube has a higher frictional pressure drop especially at the vapour qualities of 75% and 90% for mass fluxes of 300 kg/m^{2}s and 400 kg/m^{2}s. This may be attributed to the fact that the momentum pressure drop of the smooth tube was lower than that of the enhanced tube at those test conditions.

The variations of the pressure penalty factor in terms of the inclination angle, vapour quality for different mass fluxes of a) 200 kg/m^{2}s, b) 300 kg/m^{2}s and c) 400 kg/m^{2}s are shown in Fig. 25. For inclination angle of 0^o, it has been shown that the pressure drop penalty factor decreases with increasing vapor quality for all mass fluxes; this is because the augmentation due to the effect of the fins is reduced as vapour quality increases. Similar trends were obtained by Graham et al. [94] An overview of the result shows that lower pressure penalty factors are obtained during the downward and the upward flows. It can also be seen that in some instances, a pressure penalty factor lower than unity is obtained. This occurs when the frictional pressure drop of the microfin is lower than that of the smooth tube. This can be observed mostly during flows with qualities equal to or greater than 75% having the lowest performance of 0.79 for quality of 90%, mass flux of 300 kg/m^{2}s when the flow is vertically upwards. The generally low pressure penalty data obtained for mass flux of 400 kg/m^{2}s, quality of 0.9 may be due to the level of reliable resolution of the experiment's pressure transducer.

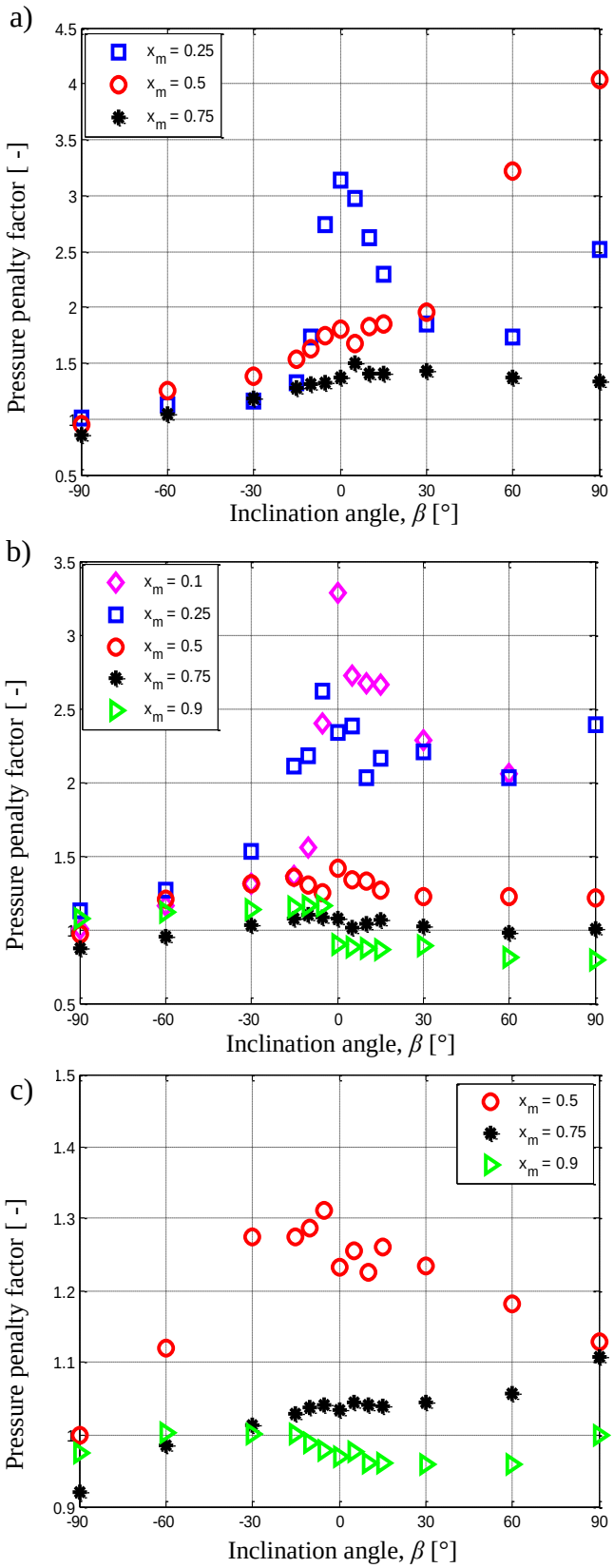

Fig. 25. Effect of inclination angle on the frictional pressure factor for different vapour qualities for mass fluxes of a) 200 kg/m^{2}s, b) 300 kg/m^{2}s and c) 400 kg/m^{2}s.

On the average, higher pressure penalty factors are obtained either during the vertical upward or near-horizontal flows. Desirable low-pressure factors are observed during the downward flow. A frictional pressure drop penalty factor of up to approximately 4.1 can be seen during the upward vertical flow for a quality of 50% and a mass flux of 200 kg/m^{2}s, and up to 3.3 during the horizontal flow for a quality of 10% and a mass flux of 300 kg/m^{2}s. For a mass flux of 400 kg/m^{2}s and quality greater than 50%, the highest pressure penalty is 1.32. Figs. 26 and 27 present the pressure penalty factor as a function of the mass flux and mean vapour quality. Fig. 26 reveals the relationship between the mass flux and the pressure penalty factor for different inclination angles for mean vapour quality of a) 25% and 90%, b) 50% and 75%. High PFs are observed for mass flux of 200 kg/m^{2}s during the upward flow having its maximum at 4.1. This can be attributed to the fact that the transition of the microfin tube from stratified-wavy flow to annular flow occurred around a mass flux of 200 kg/m^{2}s. This finding is also similar to the findings of Li et al. [41], who found their largest PF values near a mass flux of 190 kg/m^{2}s.

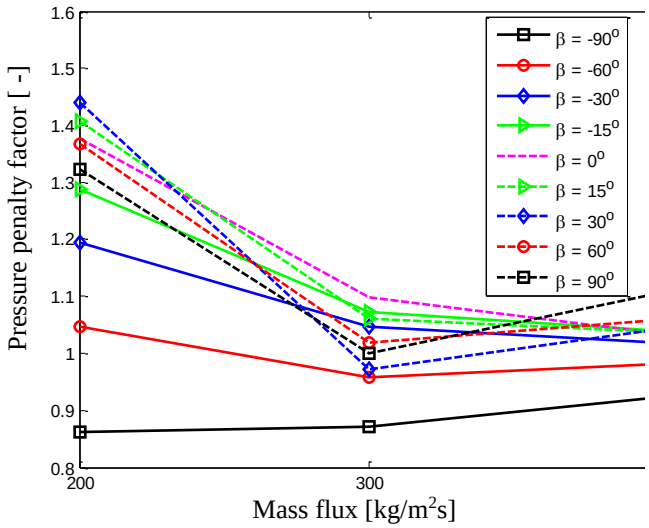

Fig. 26. Effect of mass flux on the pressure penalty factor for different inclination angles for vapour qualities of a) 25% and 90%, b) 50% and c) 75%.

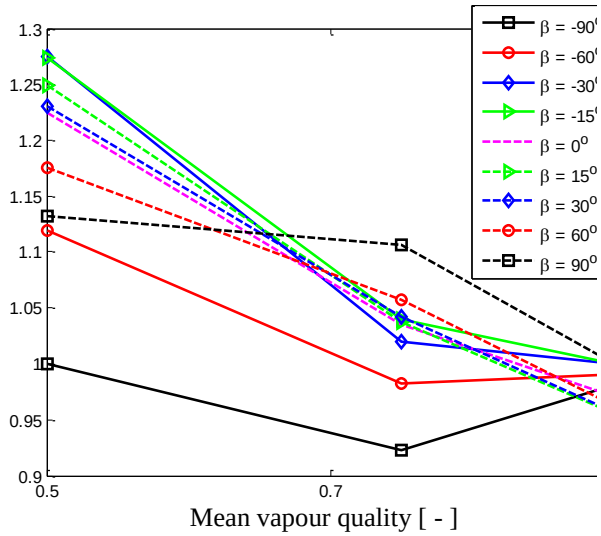

Fig. 27. Effect of mean vapour quality on the pressure penalty factor for different inclination angles for mass fluxes of a) 200 kg/m^{2}s, b) 300 kg/m^{2}s and c) 400 kg/m^{2}s.

The effect of the mean vapour quality is shown in Fig. 27 for mass flux of a) 200 kg/m^{2}s, b) 300 kg/m^{2}s and c) 400 kg/m^{2}s. For mass flux of 200 kg/m^{2}s, the trend seems unpredictable but for the mass flux of 300 kg/m^{2}s and 400 kg/m^{2}s, there is a general decrease in enhancement with an increase

in vapour quality. In comparison with the heat transfer enhancement factor, the trends are reversed. On average, the enhancement factor is higher during the downward flow than during the vertical and horizontal flows. Like the penalty factor, the enhancement factor of less than unity is obtained; in this case, it occurred only during the upward flow. EF decreases with increasing mass flux, which means that the enhancement induced by the microfins may not be very significant at high mass fluxes. Comparing the heat transfer EF with the pressure PF, it can be seen that the penalty factors at some points are higher than the enhancement factors (particularly at high mass flux and high vapour qualities). Similar assertions were reported in Wu et al. [28], Diani et al. [95], Zhang et al. [35] and Han et al. [20].

7. Conclusions

This paper presented the influences of the mean vapour quality, mass flux and inclination angle on the heat transfer coefficient and pressure drop during the condensation of R134a in a helical microfin copper tube with a helix angle of 14^{o} and a mean inner diameter of 8.92 mm. Experimental results were compared with the heat transfer coefficient and pressure drop results obtained with a smooth tube having an inner diameter of 8.38 mm. Cases with vapour qualities ranging from 10% to 90%, mass fluxes ranging from 200 kg/m^2 to 600 kg/m^2, inclination angles from -90° (downward flow) to +90° (upward flow) and saturation temperature of 40 °C were considered.

1). In general, increased mean vapour quality and mass fluxes resulted in increased heat transfer coefficients and pressure drops for both the microfin tube and the smooth tube.

2). For the microfin tube, higher heat transfer coefficients were obtained during the downward flow orientation (i.e. from -90° to 0°) than during upward flow orientations.

3). The inclination angle which resulted in the highest heat transfer coefficients was between -15° (downward flow) and -5° (downward flow) for the microfin tube, while it was either -15° (downward flow) or -30° (downward flow) for the smooth tube.

4). When compared with the heat transfer coefficients obtained with a smooth tube having a similar diameter at the same operating conditions, heat transfer enhancement factors of between 0.79 and 2.38 were obtained depending on the inclination angle, mean vapour quality and mass flux.

5). While there was a significant difference in the frictional pressure drop between the microfin and smooth tubes, there was little difference in the void fraction except for very low vapour qualities.

6). Lower pressure penalty factors were obtained during the downward flow than during horizontal and upward flows; however, a penalty factor of lower than unity was obtained for vapour quality above 50%.

Acknowledgement

The funding obtained from the NRF, TESP, Stellenbosch University/University of Pretoria, SANERI/SANEDI, CSIR, EEDSM Hub and NAC is acknowledged and duly appreciated.

References

[1] A. Cavallini, G. Censi, D. Del Col, L. Doretti, G. Longo, L. Rossetto, C. Zilio, Condensation inside and outside smooth and enhanced tubes—a review of recent research, International Journal of Refrigeration, 26 (2003) 373-392.
[2] A. Dalkilic, S. Wongwises, Intensive literature review of condensation inside smooth and enhanced tubes, International Journal of Heat and Mass Transfer, 52 (2009) 3409-3426.
[3] T. Newell, R. Shah, An assessment of refrigerant heat transfer, pressure drop, and void fraction effects in microfin tubes, HVAC&R Research, 7 (2001) 125-153.
[4] S. Lips, J.P. Meyer, Two-phase flow in inclined tubes with specific reference to condensation: A review, International Journal of Multiphase Flow, 37 (2011) 845-859.
[5] T. Naulboonrueng, J. Kaewon, S. Wongwises, Two-phase condensation heat transfer coefficients of HFC–134a at high mass flux in smooth and micro-fin tubes, International communications in heat and mass transfer, 30 (2003) 577-590.
[6] M. Akhavan-Behabadi, R. Kumar, S. Mohseni, Condensation heat transfer of R-134a inside a microfin tube with different tube inclinations, International Journal of Heat and Mass Transfer, 50 (2007) 4864-4871.
[7] S. Lips, J.P. Meyer, Experimental study of convective condensation in an inclined smooth tube. Part I: Inclination effect on flow pattern and heat transfer coefficient, International Journal of Heat and Mass Transfer, 55 (2012) 395-404.
[8] S. Lips, J.P. Meyer, Experimental study of convective condensation in an inclined smooth tube. Part II: Inclination effect on pressure drop and void fraction, International Journal of Heat and Mass Transfer, 55 (2012) 405--412.
[9] S. Lips, J.P. Meyer, Effect of gravity forces on heat transfer and pressure drop during condensation of R134a, Microgravity Science and Technology, 24 (2012) 157-164.
[10] J.P. Meyer, J. Dirker, A.O. Adelaja, Condensation heat transfer in smooth inclined tubes for R134a at different saturation temperatures, International Journal of Heat and Mass Transfer, 70 (2014) 515-525.

[11] A.O. Adelaja, J. Dirker, J.P. Meyer, Convective condensation heat transfer of R134a in tubes at different inclination angles, International Journal of Green Energy, 13 (2016) 812-821.
[12] A.O. Adelaja, D.R.E. Ewim, J. Dirker, J.P. Meyer, Experimental investigation on pressure drop and friction factor in tubes at different inclination angles during the condensation of R134a, in: Proceedings of the 15th International Heat Transfer Conference, Kyoto, Paper IHTC15-9363, 2014, pp. 10-15.
[13] S. Eckels, M. Pate, Evaporation and Condensation of HFC-134 a and CFC-12 in a Smooth Tube and a Micro-Fin Tube, ASHRAE Trans, 97 (1991).
[14] L. Chamra, R. Webb, M. Randlett, Advanced micro-fin tubes for condensation, International journal of heat and mass transfer, 39 (1996) 1839-1846.
[15] S.J. Eckels, B.A. Tesene, A comparison of R-22, R-134a, R-410A, and R-407C condensation performance in smooth and enhanced tubes: Part II, pressure drop, ASHRAE Transactions, 105 (1999) 442.
[16] A. Cavallini, D. Del Col, L. Doretti, G. Longo, L. Rossetto, Heat transfer and pressure drop during condensation of refrigerants inside horizontal enhanced tubes, International Journal of Refrigeration, 23 (2000) 4-25.
[17] A. Miyara, Y. Otsubo, S. Ohtsuka, Y. Mizuta, Effects of fin shape on condensation in herringbone microfin tubes, International journal of refrigeration, 26 (2003) 417-424.
[18] T. Nualboonrueng, S. Wongwises, Two-phase flow pressure drop of HFC-134a during condensation in smooth and micro-fin tubes at high mass flux, International communications in heat and mass transfer, 31 (2004) 991-1004.
[19] J.A. Olivier, L. Liebenberg, M.A. Kedzierski, J.P. Meyer, Pressure drop during refrigerant condensation inside horizontal smooth, helical microfin, and herringbone microfin tubes, Journal of Heat Transfer, 126 (2004) 687-687.
[20] D. Han, K.J. Lee, Experimental study on condensation heat transfer enhancement and pressure drop penalty factors in four microfin tubes, International Journal of Heat and Mass Transfer, 48 (2005) 3804-3816.
[21] H. Honda, A. Wijayanta, N. Takata, Condensation of R407C in a horizontal microfin tube, International journal of refrigeration, 28 (2005) 203-211.
[22] L. Liebenberg, J.P. Meyer, The characterization of flow regimes with power spectral density distributions of pressure fluctuations during condensation in smooth and micro-fin tubes, Experimental Thermal and Fluid Science, 31 (2006) 127-140.
[23] J.A. Olivier, L. Liebenberg, J.R. Thome, J.P. Meyer, Heat transfer, pressure drop, and flow pattern recognition during condensation inside smooth, helical micro-fin, and herringbone tubes, International Journal of Refrigeration, 30 (2007) 609-623.
[24] Y.J. Kim, J. Jang, P.S. Hrnjak, M.S. Kim, Adiabatic horizontal and vertical pressure drop of carbon dioxide inside smooth and microfin tubes at low temperatures, Journal of Heat Transfer, 130 (2008) 111001.
[25] S. Sapali, P.A. Patil, Heat transfer during condensation of HFC-134a and R-404A inside of a horizontal smooth and micro-fin tube, Experimental Thermal and Fluid Science, 34 (2010) 1133-1141.
[26] P.A. Patil, S. Sapali, Condensation pressure drop of HFC-134a and R-404A in a smooth and micro-fin U-tube, Experimental Thermal and Fluid Science, 35 (2011) 234-242.
[27] L. Colombo, A. Lucchini, A. Muzzio, Flow patterns, heat transfer and pressure drop for evaporation and condensation of R134A in microfin tubes, International Journal of Refrigeration, 35 (2012) 2150-2165.
[28] Z. Wu, B. Sundén, L. Wang, W. Li, Convective condensation inside horizontal smooth and microfin tubes, Journal of Heat Transfer, 136 (2014).
[29] A. Cavallini, D. Del Col, S. Mancin, L. Rossetto, Condensation of pure and near-azeotropic refrigerants in microfin tubes: A new computational procedure, International Journal of Refrigeration, 32 (2009) 162-174.
[30] M. Kedzierski, J. Goncalves, Horizontal convective condensation of alternative refrigerants within a micro-fin tube, Journal of Enhanced Heat Transfer, 6 (1999).
[31] L.M. Chamra, P.J. Mago, M.O. Tan, C.C. Kung, Modeling of condensation heat transfer of pure refrigerants in micro-fin tubes, International Journal of Heat and Mass Transfer, 48 (2005) 1293-1302.
[32] J. Yu, S. Koyama, Condensation heat transfer of pure refrigerants in microfin tubes, in: International Refrigeration Conference, Purdue, West Lafayette, 1998, pp. 325-330.
[33] J. Zhang, W. Li, W. Minkowycz, Numerical simulation of R410A condensation in horizontal microfin tubes, Numerical Heat Transfer, Part A: Applications, 71 (2017) 361-376.

[34] G. Li, L. Huang, L. Tao, Experimental investigation of refrigerant condensation heat transfer characteristics in the horizontal microfin tubes, Applied Thermal Engineering, 123 (2017) 1484-1493.
[35] J. Zhang, N. Zhou, W. Li, Y. Luo, S. Li, An experimental study of R410A condensation heat transfer and pressure drops characteristics in microfin and smooth tubes with 5 mm OD, International Journal of Heat and Mass Transfer, 125 (2018) 1284-1295.
[36] M.K. Bashar, K. Nakamura, K. Kariya, A. Miyara, Experimental study of condensation heat transfer and pressure drop inside a small diameter microfin and smooth tube at low mass flux condition, Applied Sciences, 8 (2018) 2146.
[37] Z.-c. Sun, W. Li, A new general correlation for frictional pressure drop during condensation inside horizontal micro-fin tubes, International Journal of Heat and Mass Transfer, 112 (2017) 587-596.
[38] A. Cavallini, D. Del Col, L. Doretti, G. Longo, L. Rossetto, Pressure drop during condensation and vaporization of refrigerants inside enhanced tubes, Heat and technology, 15 (1997) 3-10.
[39] Y. Yang, L. Jia, Q. Peng, Investigation on condensation heat transfer and pressure drop of R410A during upward flow in vertical smooth and micro-fin tube, International Journal of Heat and Mass Transfer, 108 (2017) 2293-2302.
[40] L.M. Chamra, P.J. Mago, Modeling of condensation heat transfer of refrigerant mixture in micro-fin tubes, International Journal of Heat and Mass Transfer, 49 (2006) 1915-1921.
[41] W. Li, W. Tang, J. Chen, H. Zhu, D.J. Kukulka, Y. He, Z. Sun, J. Du, B. Zhang, Convective condensation in three enhanced tubes with different surface modifications, Experimental Thermal and Fluid Science, 97 (2018) 79-88.
[42] Q.V. Pham, K.-I. Choi, J.-T. Oh, H. Cho, Flow condensing heat transfer of R410A, R22, and R32 inside a micro-fin tube, Experimental Heat Transfer, 32 (2019) 102-115.
[43] A.O. Adelaja, J. Dirker, J.P. Meyer, Condensing heat transfer coefficients for R134a at different saturation temperatures in inclined tubes, in: Proceedings of the ASME2013 Heat Transfer Summer Conference, HT2013, Paper number: HT2013-17375, Minneapolis, 2013, pp. 14-19.
[44] A.O. Adelaja, J. Dirker, J.P. Meyer, Experimental study of the pressure drop during condensation in an inclined smooth tube at different saturation temperatures, International Journal of Heat and Mass Transfer, 105 (2017) 237-251.
[45] S.P. Olivier, J.P. Meyer, M. De Paepe, K. De Kerpel, The influence of inclination angle on void fraction and heat transfer during condensation inside a smooth tube, International Journal of Multiphase Flow, 80 (2016) 1-14.
[46] L. Liebenberg, J.P. Meyer, Refrigerant condensation flow regimes in enhanced tubes and their effect on heat transfer coefficients and pressure drops, Heat Transfer Engineering, 29 (2008) 506-520.
[47] L. Liebenberg, J.P. Meyer, A review of flow pattern-based predictive correlations during refrigerant condensation in horizontally smooth and enhanced tubes, Heat Transfer Engineering, 29 (2008) 3-19.
[48] L. Liebenberg, J.R. Thome, J.P. Meyer, Flow visualization and flow pattern identification with power spectral density distributions of pressure traces during refrigerant condensation in smooth and microfin tubes, Journal of Heat Transfer, 127 (2005) 209-220.
[49] J. Olivier, J.P. Meyer, Single-phase heat transfer and pressure drop of the cooling of water inside smooth tubes for transitional flow with different inlet geometries (RP-1280), HVAC&R Research, 16 (2010) 471-496.
[50] R. Suliman, L. Liebenberg, J.P. Meyer, Improved flow pattern map for accurate prediction of the heat transfer coefficients during condensation of R-134a in smooth horizontal tubes and within the low-mass flux range, International Journal of Heat and Mass Transfer, 52 (2009) 5701-5711.
[51] H. Canière, C. T'Joen, A. Willockx, M. De Paepe, M. Christians, E. Van Rooyen, L. Liebenberg, J. Meyer, Horizontal two-phase flow characterization for small diameter tubes with a capacitance sensor, Measurement Science and Technology, 18 (2007) 2898.
[52] D.R.E. Ewim, J.P. Meyer , S.M.A. Noori Rahim Abadi, Condensation heat transfer coefficients in an inclined smooth tube at low mass fluxes, International Journal of Heat and Mass Transfer, 123 (2018) 455-467.
[53] J.P. Meyer, D.R.E. Ewim, Heat transfer coefficients during the condensation of low mass fluxes in smooth horizontal tubes, International Journal of Multiphase Flow, 99 (2018) 485-499.
[54] D.R.E. Ewim, R. Kombo, J.P. Meyer, Flow pattern and experimental investigation of heat transfer coefficients during the condensation of R134a at low mass fluxes in a smooth horizontal tube, in: 12th

International Conference on Heat Transfer, Fluid Mechanics and Thermodynamics (HEFAT), Costa del Sol, Malaga, Spain, 2016, pp. 264-269.
[55] D.R.E. Ewim, J.P. Meyer, Pressure drop during condensation at low mass fluxes in smooth horizontal and inclined tubes, International Journal of Heat and Mass Transfer, 133 (2019) 686-701.
[56] R. Rayle, Influence of orifice geometry on static pressure measurements, American Society of Mechanical Engineers, 1959.
[57] E. Van Rooyen, Time-fractional analysis of flow patterns during refrigerant condensation, M.Eng. Thesis, in: Mechanical and Aeronautical Engineering, University of Pretoria, 2007.
[58] E.W. Lemmon, M.L. Huber, M.O. McLinden, NIST standard reference database 23: reference fluid thermodynamic and transport properties (REFPROP), version 9.1, National Institute of Standards and Technology, Standard reference data program, Gaithersburg, (2013).
[59] ASHRAE, ASHRAE Standard 41.4: Method for measurement of proportion of lubricant in liquid refrigerant, in, American Society for Heating, Refrigeration, and Air-conditioning Engineers, USA, 2006.
[60] M.B. Ould Didi, N. Kattan, J.R. Thome, Prediction of two-phase pressure gradients of refrigerants in horizontal tubes, International Journal of Refrigeration, 25 (2002) 935-947.
[61] W. Zhang, T. Hibiki, K. Mishima, Correlations of two-phase frictional pressure drop and void fraction in mini-channel, International Journal of Heat and Mass Transfer, 53 (2010) 453-465.
[62] A. Cioncolini, J.R. Thome, Void fraction prediction in annular two-phase flow, International Journal of Multiphase Flow, 43 (2012) 72-84.
[63] S.Z. Rouhani, E. Axelsson, Calculation of void volume fraction in the subcooled and quality boiling regions, International Journal of Heat and Mass Transfer, 13 (1970) 383-393.
[64] S.M. Bhagwat, A.J. Ghajar, A flow pattern independent drift flux model based void fraction correlation for a wide range of gas-liquid two phase flow, International Journal of Multiphase Flow, 59 (2014) 186-205.
[65] M.M. Shah, Prediction of heat transfer during condensation in inclined plain tubes, Applied Thermal Engineering, 94 (2016) 82-89.
[66] A. Cavallini, D.D. Col, L. Doretti, M. Matkovic, L. Rossetto, C. Zilio, G. Censi, Condensation in horizontal smooth tubes: A new heat transfer model for heat exchanger design, Heat Transfer Engineering, 27 (2006) 31-38.
[67] M.M. Shah, A general correlation for heat transfer during film condensation inside pipes, International Journal of Heat and Mass Transfer, 22 (1979) 547-556.
[68] M.M. Shah, General correlation for heat transfer during condensation in plain tubes: further development and verification, ASHRAE Transactions, 119 (2013) 3.
[69] A. Cavallini, G. Censi, D.D. Col, L. Doretti, L. Rossetto, G.A. Longo, Heat transfer coefficients of HFC refrigerants during condensation at high temperature inside an enhanced tube, in: 9th International Refrigeration and Air Conditioning Conference, Purdue, USA, 2002, pp. Paper 563.
[70] J. Thome, Engineering Data Book III, Huntsville, AL: Wolverine Tube, in, Inc, 2006.
[71] S. Zivi, Estimation of steady-state steam void-fraction by means of the principle of minimum entropy production, Journal of heat transfer, 86 (1964) 247-251.
[72] G.B. Wallis, One-dimensional two-phase flow, McGraw-Hill, New York, NY, 1969.
[73] J. Chen, A further examination of void fraction in annular two-phase flow, International journal of heat and mass transfer, 29 (1986) 1760-1763.
[74] D.A. Yashar, M. Wilson, H. Kopke, D. Graham, J. Chato, T. Newell, An investigation of refrigerant void fraction in horizontal, microfin tubes, Hvac&R Research, 7 (2001) 67-82.
[75] D. Graham, H. Kopke, M. Wilson, D. Yashar, J. Chato, T. Newell, An Investigation of Void Fraction in the Annular/Stratified Flow Regions in Smooth, Horizontal Tubes ACRC TR-144, Air Conditioning and Refrigeration Center, University of Illinois, Urbana, USA, (1998).
[76] H.R. Kopke, Experimental investigation of void fraction during refrigerant condensation in horizontal tubes, in, Air Conditioning and Refrigeration Center. College of Engineering. University of Illinois at Urbana-Champaign., 1998.
[77] M.J. Wilson, Experimental investigation of void fraction during horizontal flow in larger diameter refrigeration applications, in, Air Conditioning and Refrigeration Center. College of Engineering. University of Illinois at Urbana-Champaign., 1998.
[78] L. Friedel, Improved friction pressure drop correlation for horizontal and vertical two-phase pipe flow,

Proc. of European Two-Phase Flow Group Meet., Ispra, Italy, 1979, (1979).
[79] R. Grönnerud, Investigation of liquid hold-up, flow-resistance and heat transfer in circulation type evaporators, part IV: two-phase flow resistance in boiling refrigerants, Bull. De l'Inst. Du Froid, Annexe, 1 (1972).
[80] R.W. Lockhart, R.C. Martinelli, Proposed correlation of data for isothermal, two-phase, two-component flow in pipes, Chemical Engineering Progress Symposium Series, 45 (1949) 39-48.
[81] D. Chisholm, Pressure gradients due to friction during the flow of evaporating two-phase mixtures in smooth tubes and channels, International Journal of Heat and Mass Transfer, 16 (1973) 347-358.
[82] H. Müller-Steinhagen, K. Heck, A simple friction pressure drop correlation for two-phase flow in pipes, Chemical Engineering and Processing: Process Intensification, 20 (1986) 297-308.
[83] J. Choi, M.A. Kedzierski, P.A. Domanski, Generalized pressure drop correlation for evaporation and condensation in smooth and micro-fin tubes, Proceedings of IIF-IIR Commission B, 1 (2001) 9-16.
[84] H. Liu, C.O. Vandu, R. Krishna, Hydrodynamics of Taylor flow in vertical capillaries: flow regimes, bubble rise velocity, liquid slug length, and pressure drop, Industrial & engineering chemistry research, 44 (2005) 4884-4897.
[85] P. Spedding, E. Bénard, Gas–liquid two phase flow through a vertical 90 elbow bend, Experimental Thermal and fluid science, 31 (2007) 761-769.
[86] M. Zangana, G. Van der Meulen, B. Azzopardi, The effect of gas and liquid velocities on frictional pressure drop in two phase flow for large diameter vertical pipe, in: 7th International Conference on Multiphase Flow, ICMF, 2010.
[87] K. Mishima, T. Hibiki, Some characteristics of air-water two-phase flow in small diameter vertical tubes, International Journal of Multiphase Flow, 22 (1996) 703-712.
[88] K. Cornwell, P.A. Kew, Boiling in small parallel channels, in: Energy Efficiency in Process Technology, Springer, 1993, pp. 624-638.
[89] D. Nicklin, Two-phase bubble flow, Chemical engineering science, 17 (1962) 693-702.
[90] S.G. Kandlikar, Two-phase flow patterns, pressure drop, and heat transfer during boiling in minichannel flow passages of compact evaporators, Heat Transfer Engineering, 23 (2002) 5-23.
[91] H. Wang, H. Honda, Condensation of refrigerants in horizontal microfin tubes: comparison of prediction methods for heat transfer, International Journal of Refrigeration, 26 (2003) 452-460.
[92] R.J. Moffat, Describing the uncertainties in experimental results, Experimental Thermal and Fluid Science, 1 (1988) 3-17.
[93] J.-P.M. Bukasa, L. Liebenberg, J.P. Meyer, Heat transfer performance during condensation inside spiralled micro-fin tubes, Journal of heat transfer, 126 (2004) 321-328.
[94] D. Graham, J. Chato, T. Newell, Heat transfer and pressure drop during condensation of refrigerant 134a in an axially grooved tube, International journal of heat and mass transfer, 42 (1999) 1935-1944.
[95] A. Diani, A. Cavallini, L. Rossetto, R1234yf condensation inside a 3.4 mm ID horizontal microfin tube, International Journal of Refrigeration, 75 (2017) 178-189.